NEUROSCIENCE

Coordinated activity of a central pathway drives associative opioid analgesic tolerance

Yiwen Hou[1]†, Guichang Zou[1,2]†, Xianglian Wang[1], Hui Guo[1], Xiao Ma[1], Xingyu Cheng[3], Zhiyong Xie[3], Xin Zuo[1], Jing Xia[1], Huanhuan Mao[1], Man Yuan[1], Qi Chen[1], Peng Cao[3], Yupeng Yang[1], Li Zhang[4], Wei Xiong[1,2,5]*

Opioid analgesic tolerance, a root cause of opioid overdose and misuse, can develop through an associative learning. Despite intensive research, the locus and central pathway subserving the associative opioid analgesic tolerance (AOAT) remains unclear. Using a combination of chemo/optogenetic manipulation with calcium imaging and slice physiology, here we identify neuronal ensembles in a hierarchically organized pathway essential for AOAT. The association of morphine-induced analgesia with an environmental condition drives glutamatergic signaling from ventral hippocampus (vHPC) to dorsomedial prefrontal cortex (dmPFC) cholecystokininergic (CCKergic) neurons. Excitation of CCKergic neurons, which project and release CCK to basolateral amygdala (BLA) glutamatergic neurons, relays AOAT signal through inhibition of BLA μ-opioid receptor function, thereby leading to further loss of morphine analgesic efficacy. This work provides evidence for a circuit across different brain regions distinct for opioid analgesic tolerance. The components of this pathway are potential targets to treat opioid overdose and abuse.

INTRODUCTION

Opioids are not only the most effective analgesics to relieve pain but also among the most abusive substances to cause social and economic crisis (*1*–*3*). Opioid tolerance is one primary root cause of physical dependence, withdrawal, and overdoses (*4*). Tolerance develops to the analgesic effects of opioid agonists such as morphine and fentanyl in the treatment of human chronic pain. Escalating opioid use up to more than 10-fold dose is a common practice to resist against tolerance and achieve the desired effect (*5*–*7*). A major interest of opioid research in the past several decades is to develop ideal agonists that target μ-opioid receptors (MORs) with a high analgesic efficacy and a delayed development of tolerance (*7*–*10*). Despite intensive research, the attempt in this research direction has been substantially hindered because the neurological mechanisms underlying opioid analgesic tolerance in the brain remain unclear. Research on this topic has been carried out mainly in vitro and focused on posttranslational modification of opioid receptors and their signaling cascades at the cellular level (*11*–*13*). However, there is a serious lack of experimental data uncovering the central pathways that specifically regulate the development of tolerance to the analgesic effect of opioids.

Accumulating evidence has emerged to suggest that learning processes play an essential role in the development of tolerance to the analgesic effect of opioids. For instance, a large amount of animal studies show that rodents administered with morphine in a distinctive context displayed a higher degree of morphine tolerance than the animals given morphine in a home cage (*14*–*20*). This associative opioid analgesic tolerance (AOAT) can also make a clinical impact on the analgesic efficacy in the treatment of patients with chronic pain (*21*). Opioid users developed with AOAT became supersensitive and even life-threatened to nonlethal doses of morphine in the absence of experienced context (*22*–*24*).

Previous studies have demonstrated that cholecystokinin (CCK), the most effective endogenous anti-opioid peptide (*25*), is colocalized with endogenous opioids and opioid receptors in various pain-processing brain regions (*26*, *27*). Although CCK does not bind to opioid receptors (*28*), its binding to CCK receptors reduces the binding affinity of opioids to opioid receptors (*28*, *29*). Considerable experimental evidence also show that CCK diminished the analgesic effect of opioids such as morphine, heroin, and beta-endorphin (*25*, *30*–*32*). Systemic or intracerebral administration of CCK receptor antagonists proglumide and L365260, as well as CCK8 antiserum, potentiated the analgesic effects of opioids and impeded the development of opioid analgesic tolerance (*33*–*41*). Furthermore, an early investigation suggests that associative morphine tolerance is mediated in a CCK-2 receptor (CCK2R)–dependent mechanism in amygdala (*16*). Until recently, little is known about the neuronal circuit in the brain that underlies opioid analgesic tolerance. To address this question, we implemented in vivo techniques involving optogenetic and chemogenetic manipulations, neuronal calcium imaging, and electrophysiological recording to explore a brain pathway and its functional and structural elements for regulation of AOAT. We have provided evidence for a distinct neuronal circuitry and its hierarchical control of the development of tolerance to the analgesic effect of opioids in the brain. We have further dissected the functional elements that sequentially relay the signals across the Glu^{vHPC}→CCK^{dmPFC}→Glu^{BLA} pathway. This neuronal circuit is the target in the brain to drive AOAT.

[1]Department of Neurology, The First Affiliated Hospital of USTC, Division of Life Sciences and Medicine, Hefei National Research Center for Physical Sciences at the Microscale, University of Science and Technology of China, Hefei 230026, China. [2]Institute of Artificial Intelligence, Hefei Comprehensive National Science Center, Hefei 230088, China. [3]National Institute of Biological Sciences, Beijing 102206, China. [4]Laboratory for Integrative Neuroscience, National Institute on Alcohol Abuse and Alcoholism, National Institutes of Health, Bethesda, MD 20892, USA. [5]Anhui Province Key Laboratory of Biomedical Aging Research, Hefei 230026, China.
†These authors contributed equally to this work.
*Corresponding author. Email: wxiong@ustc.edu.cn

RESULTS

Identification of discrete brain regions involving AOAT

To generate AOAT model (*16*), morphine at different doses was given to mice via intraperitoneal injection for consecutive days. Mice receiving morphine were subgrouped into two, nonconditioned home-caged mice (HC-mice) and contextual conditioned caged mice (CC-mice) (Fig. 1A). The contextual cues alone did not change the acute morphine analgesic effects (1 to 5 mg/kg) (fig. S1) or basal nociceptive sensitivity (fig. S2). Chronic systemic morphine treatments of HC-mice and CC-mice both resulted in the development of intrinsic morphine analgesic tolerance in the hot-plate tests (Fig. 1B). The tolerance development in the HC-mice is independent of context, as the development of tolerance both in mice with constantly shifted morphine injection context and in previously reported context-independent mice from a 2 × 2 crossover design (*16*) is similar with that in the HC-mice (fig. S3). However, when compared to HC-mice, CC-mice exhibited significantly accelerated morphine analgesic tolerance after repeated administration of morphine at various doses (1 to 5 mg/kg per day) (Fig. 1B and fig. S4), indicating that the AOAT model was successfully established in the CC-mice. This AOAT behavior showed no differences between male and female mice (fig. S5), suggesting that there is no sexual dimorphism of AOAT. We next examined whether this AOAT behavior also occurs in the treatment of chronic

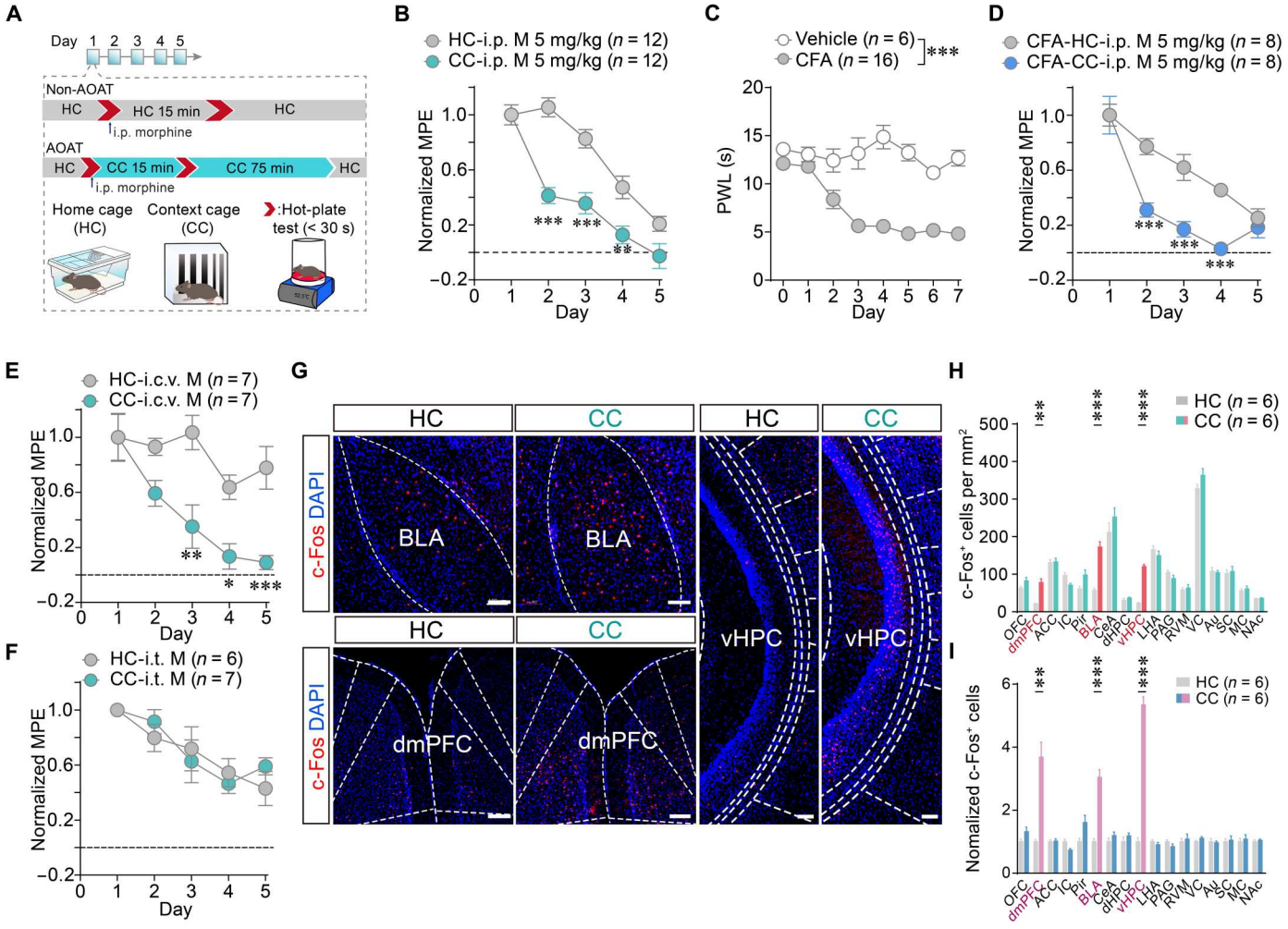

Fig. 1. Identification of brain regions critical for AOAT. (**A**) Schematic of the AOAT experimental procedure. The HC-mice received intraperitoneal (i.p.) injection of morphine in their home cage (HC), while the CC-mice received intraperitoneal injection of morphine in the context cage (CC). Hot-plate tests (within 30 s) were performed before and 15 min after morphine injection. (**B**) Morphine analgesic tolerance in the HC-mice and CC-mice. The antinociception was calculated to maximum possible effect (MPE) according to the equation: MPE = [Post-drug PWL (s) − Pre-drug PWL (s)]/[Cutoff time (s) − Pre-drug PWL (s)]. (**C**) Quantitative paw withdrawal latency (PWL) of mice in hot-plate tests before and after CFA (20 μl, 50%) or vehicle bilateral intraplantar injection. (**D**) Morphine analgesic tolerance in the CFA-treated HC-mice and CC-mice. (**E** and **F**) Morphine analgesic tolerance in the HC-mice and CC-mice receiving intracerebroventricular (i.c.v.) (E; 3 μg per mice) or intrathecal (i.t.) (F; 0.3 μg per mice) morphine delivery. (**G**) Representative images of c-Fos immunofluorescence staining in BLA, dmPFC, and vHPC of HC-mice and CC-mice. DAPI, 4′, 6-diamidino-2-phenylindole. Scale bars, 100 μm. (**H**) Quantification of the number of c-Fos$^+$ neurons in the HC group and the CC group ($n = 6$ mice per group). (**I**) The number of c-Fos$^+$ neurons in the CC group was normalized to the HC group in each nucleus. OFC, orbitofrontal cortex; dmPFC, dorsomedial prefrontal cortex; ACC, anterior cingulate cortex; IC, insular cortex; Pir, piriform cortex; BLA, basolateral amygdala; CeA, central amygdala; dHPC, dorsal hippocampus; vHPC, ventral hippocampus; LHA, lateral hypothalamic area; PAG, periaqueductal gray; RVM, rostral ventromedial medulla; VC, visual cortex; Au, auditory cortex; SC, somatosensory cortex; MC, motor cortex; NAc, nucleus accumbens. Data are presented as means ± SEM. *$P < 0.05$, **$P < 0.01$, and ***$P < 0.001$ by two-way ANOVA with Bonferroni post hoc test; ns, not significant ($P > 0.05$).

inflammatory pain. The mice received bilateral intraplantar injection of complete Freund's adjuvant (CFA) (*42*) and exhibited progressive thermal hyperalgesia over the next 7 days (Fig. 1C). AOAT also developed during the treatment of CFA-induced chronic pain in CC-mice, but not HC-mice (Fig. 1D and fig. S6). This AOAT behavior was also produced by repeated exposure to systemic sufentanil (intraperitoneally, 35 μg/kg per day for 5 days), a currently widely used synthetic opioid analgesic in clinic (fig. S7).

We next asked whether AOAT is formed at the spinal or supraspinal level since both areas can mediate opioid analgesia and analgesic tolerance (*43*). We observed that CC-mice receiving intracerebroventricular, but not intrathecal, microinjection of morphine exhibited AOAT, favoring a supraspinal pathway involving AOAT (Fig. 1, E and F, and fig. S8). To further identify the discrete brain regions responding to AOAT, we then examined the expression of the immediate early gene *c-Fos* (a marker of recent neuronal activity) in 16 different brain subregions in HC-mice and CC-mice after 5 days of repeated morphine injections. There was a substantial increase in c-Fos expression in three brain regions including basolateral amygdala (BLA), dorsomedial prefrontal cortex (dmPFC), and ventral hippocampus (vHPC) in CC-mice as compared to HC-mice (Fig. 1, G to I, and fig. S9).

Development of AOAT requires coordinated neuronal activity of a vHPC→dmPFC→BLA pathway

To explore the interrelationship between AOAT behavior and enhanced neuronal activity observed in different brain regions, we ablated neurons in vivo through caspase3-mediated induction of apoptosis. We selectively ablated neurons in BLA, dmPFC, and vHPC with intracranial injection of an AAV-flex-taCasp3-TEVp virus with an AAV-Cre virus in mice (fig. S10A). Four weeks after the injection, we tested whether AOAT phenotype depends on enhanced c-Fos expression. Ablation of BLA neurons completely abolished morphine analgesia without significantly altering AOAT-induced enhancement of c-Fos level in vHPC and dmPFC (Fig. 2, A and B, and fig. S10B). Selective ablation of dmPFC or vHPC neurons inhibited AOAT without significantly altering acute morphine analgesia (Fig. 2, D and G, and fig. S10, C and D). This suggests that AOAT develops in the upstream regions of BLA, possibly dmPFC and vHPC. We observed that ablation of dmPFC neurons inhibited AOAT enhancement of BLA c-Fos, but not vHPC c-Fos (Fig. 2E), whereas ablation of vHPC neurons blocked AOAT enhancement of c-Fos level in both dmPFC and BLA regions (Fig. 2H). Collectively, these findings suggest that AOAT develops via a hierarchical pathway, vHPC→dmPFC→BLA (Fig. 2, C, F, and I).

AOAT requires excitation of $Glu^{vHPC\rightarrow dmPFC}$ neurons

Previous reports indicate that vHPC projections to dmPFC (*44*–*46*) regulate contextual coding (*47*). In view of our above observation, we proposed that the signal of AOAT circuitry should start from vHPC and end at BLA. To test this hypothesis, we first transfected vHPC with AAV-based channelrhodopsin2 (ChR2) (Fig. 3A). The ChR2–enhanced yellow fluorescent protein–positive ($EYFP^+$) signal was substantially observed in the vHPC neuron axon terminals in dmPFC (Fig. 3B). Whole-cell recordings showed that light pulses (473 nm, 15 mW/mm^2, 5 ms) illuminating vHPC ChR2-$EYFP^+$ axon terminals evoked robust excitatory postsynaptic currents (EPSCs) in dmPFC neurons (Fig. 3C). The optically evoked EPSCs (oEPSCs) could be blocked by AMPA/kainite antagonist NBQX [2,3-dioxo-6-nitro-7-sulfamoyl-benzo(*F*)quinoxaline] with *N*-methyl-D-aspartate NMDA receptor antagonist MK801 [(+)-5-methyl-10,11-dihydroxy-5*H*-dibenzo(*a*,*d*)cyclohepten-5,10-imine] (Fig. 3C), indicating that dmPFC neurons receive an excitatory glutamatergic input from vHPC.

To explore AOAT glutamatergic signaling from vHPC to dmPFC, we retrograde-labeled the $Glu^{vHPC\rightarrow dmPFC}$ neurons to examine the neuronal activity of these neurons. AAV2-retro-DIO–enhanced green fluorescent protein (EGFP) was injected into dmPFC of vGluT2-Cre mice (Fig. 3D). Whole-cell recordings of the vHPC $EGFP^+$ neurons revealed significantly enhanced intrinsic excitability, manifested by increased action potential (AP) firing rates and a reduced current threshold (i.e., minimal injected current required to evoke AP), in CC-mice as compared to HC-mice after 3 days of repeated injections of morphine rather than saline (Fig. 3, E and F). This suggests that AOAT starts and develops with increasing $Glu^{vHPC\rightarrow dmPFC}$ neuronal activity.

To explore AOAT glutamatergic signaling from vHPC to dmPFC, we then performed chemogenetic manipulation of the $Glu^{vHPC\rightarrow dmPFC}$ projections using DREADDs (designer receptors exclusively activated by designer drugs) approach in vGluT2-Cre mice. Briefly, the vGluT2-Cre mice were given with bilateral intra-vHPC injection of AAV-DIO-hM4Di-mCherry, AAV-DIO-hM3Dq-mCherry, or AAV-DIO-mCherry (control). Two cannulas were bilaterally implanted onto the dmPFC area of the mice 3 weeks after the virus injection. Clozapine-*N*-oxide (CNO) was delivered via the cannulas to activate or inactivate the Glu^{vHPC} terminals in dmPFC before AOAT training and tests (Fig. 3G). The hM4Di/hM3Dq-mCherry signals were strictly distributed in vHPC (fig. S11, A and D). In fresh vHPC brain slices, bath application of CNO (5 μM) significantly reduced the AP firing rates and increased the spike threshold of hM4Di-$mCherry^+$ neurons (fig. S11, B and C), while the CNO had an opposite effect on hM3Dq-$mCherry^+$ neurons (fig. S11E). In dmPFC brain slices, CNO (5 μM) treatment considerably decreased or increased the frequency of spontaneous EPSCs (sEPSCs) of dmPFC neurons from the mice with vHPC infection of hM4Di or hM3Dq separately (Fig. 3, H and I). Chemogenetic inactivation of $hM4Di^+$ $Glu^{vHPC\rightarrow dmPFC}$ terminals after intra-dmPFC injection of CNO markedly suppressed AOAT. On the contrary, chemogenetic activation of $hM3Dq^+$ $Glu^{vHPC\rightarrow dmPFC}$ terminals significantly aggravated morphine analgesic tolerance in HC-mice (Fig. 3J). Neither activation nor inactivation of $Glu^{vHPC\rightarrow dmPFC}$ terminals affected the acute analgesic effects of morphine (fig. S11F). CNO has no direct effect on morphine analgesic tolerance and AOAT in normal mice (fig. S12).

We next examined whether the $Glu^{vHPC\rightarrow dmPFC}$ pathway mediates the tolerance on opioid analgesic effects to other types of pain, such as neuropathic pain. Mice were treated with ablation of S1/S2 corticospinal neurons to induce the spared nerve injury (SNI) model and exhibited progressive cold hyperalgesia over the next 10 days (fig. S13, A and B). AOAT also developed in the SNI-CC-mice but not in the SNI-HC-mice (fig. S13C). Chemogenetic inactivation of the $Glu^{vHPC\rightarrow dmPFC}$ terminals significantly suppressed AOAT development in the SNI-CC-hM4Di mice (fig. S13C) without affecting acute morphine analgesia (fig. S13D).

Previous reports have shown that some opioid addicts died following drug administered in an unusual context, although postmortem examination revealed that blood levels of opioids in these

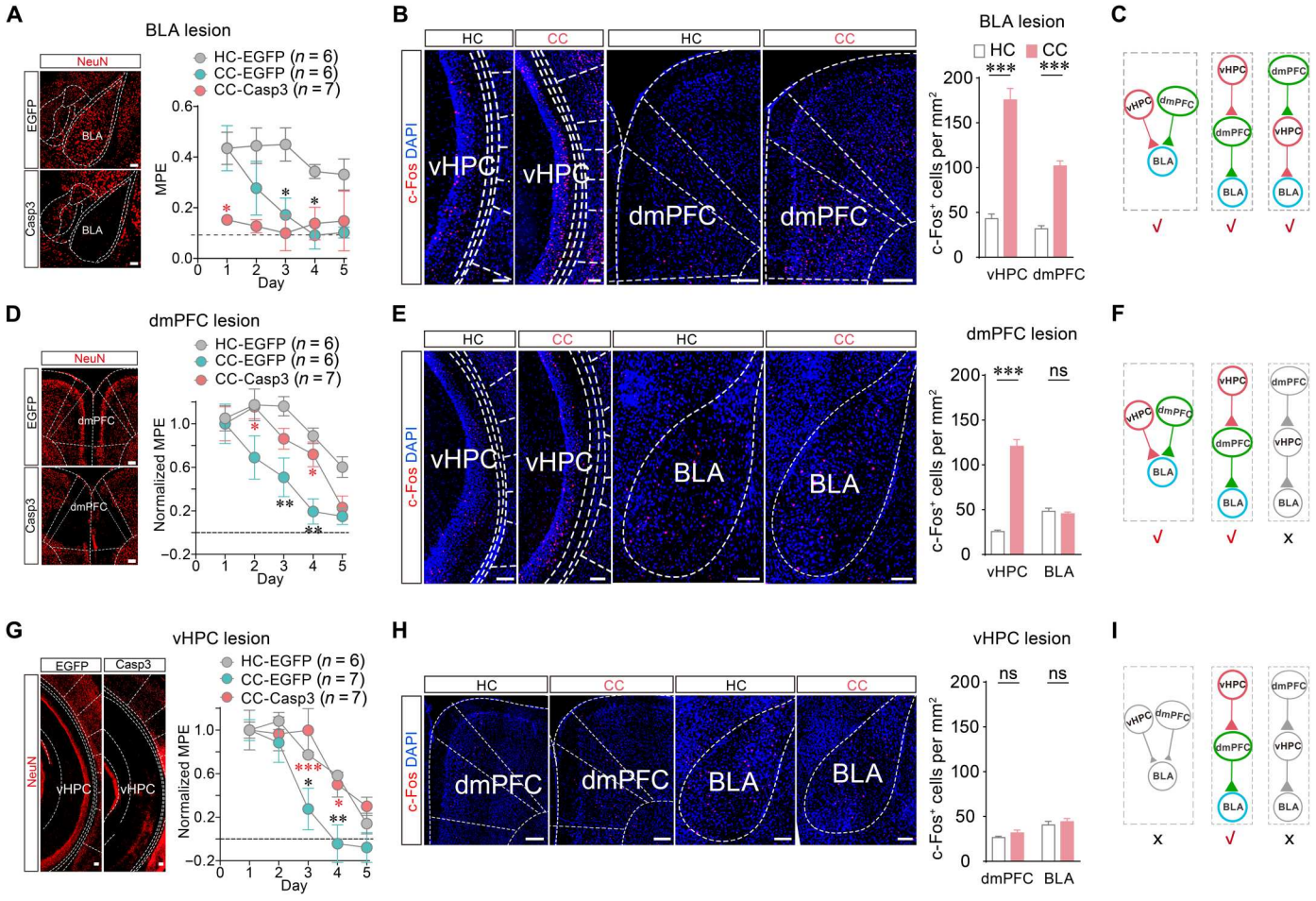

Fig. 2. Possibilities of relationships between vHPC, dmPFC, and BLA. (**A**) BLA NeuN staining (left) and development of morphine analgesic tolerance (right) in the CC-mice with or without Casp3-based ablation of BLA neurons and in the HC-mice. Scale bars, 100 μm. (**B**) Representative images (left) and quantification of the number (right) of c-Fos$^+$ neurons in vHPC and dmPFC of HC-mice and CC-mice with BLA ablation ($n = 6$ brain slices from three mice per group). Scale bars, 100 μm. (**C**) Possibilities of upstream and downstream relationships between vHPC, dmPFC, and BLA based on (A) and (B). (**D**) dmPFC NeuN staining (left) and development of morphine analgesic tolerance (right) in the CC-mice with or without Casp3-based ablation of dmPFC neurons and in the HC-mice. Scale bars, 100 μm. (**E**) Representative images (left) and quantification of the number (right) of c-Fos$^+$ neurons in vHPC and BLA of HC-mice and CC-mice with dmPFC ablation ($n = 6$ brain slices from three mice per group). Scale bars, 100 μm. (**F**) Possibilities of upstream and downstream relationships between vHPC, dmPFC, and BLA based on (A) to (E). (**G**) vHPC NeuN staining (left) and development of morphine analgesic tolerance (right) in the CC-mice with or without Casp3-based ablation of vHPC neurons and in the HC-mice. Scale bars, 100 μm. (**H**) Representative images (left) and quantification of the number (right) of c-Fos$^+$ neurons in dmPFC and BLA of HC-mice and CC-mice with vHPC ablation ($n = 6$ brain slices from three mice per group). Scale bars, 100 μm. (**I**) Possibilities of upstream and downstream relationships between vHPC, dmPFC, and BLA based on (A) to (H). Data are presented as means ± SEM. *$P < 0.05$, **$P < 0.01$, and ***$P < 0.001$ by two-way ANOVA with Bonferroni post hoc test; ns, not significant ($P > 0.05$).

addicts were not fatal (*48*). They typically died of respiratory depression because the opioids induced greater respiratory depression than expected (*18*, *49*). On the basis of these, we examined whether the morphine-induced respiratory depression could develop with associative tolerance. Briefly, mice exhibited a significantly slower respiratory rate 30 min after systemic morphine injection (10 mg/kg, intraperitoneally) (fig. S13E). Mice with or without hM4Di infection of the Glu^{vHPC} neurons received morphine (10 mg/kg, intraperitoneally) administration in HC and CC for five consecutive days. The CC-mice exhibited significantly enhanced tolerance to morphine-induced respiratory depression as compared to the HC-mice. However, the chemogenetic inactivation of the Glu$^{vHPC→dmPFC}$ terminals did not affect this enhancement of tolerance in the CC-mice (fig. S13, F and G). These findings suggest that the Glu$^{vHPC→dmPFC}$ projection selectively modulates the tolerance on opioid analgesic effects to various forms of pain.

A very recent study has provided evidence for a direct neuronal input from vHPC to BLA that contributes to generalized fear (*50*). We therefore examined whether such a vHPC→BLA pathway also regulates AOAT. We first injected AAV2-retro-mCherry into BLA to identify an anatomical connection from vHPC to BLA. In line with the previous observation, mCherry$^+$ signals were detected in vHPC 3 weeks after the viral injection (Fig. 3K). We next injected AAV2-retro-Cre into BLA and AAV-DIO-hM4Di-mCherry into vHPC to chemogenetic inactivation of the BLA-projecting vHPC neurons (Fig. 3L). However, chemogenetic inactivation of the BLA-projecting vHPC neurons induced by CNO injection (1 mg/kg, intraperitoneally) did not significantly affect AOAT and acute

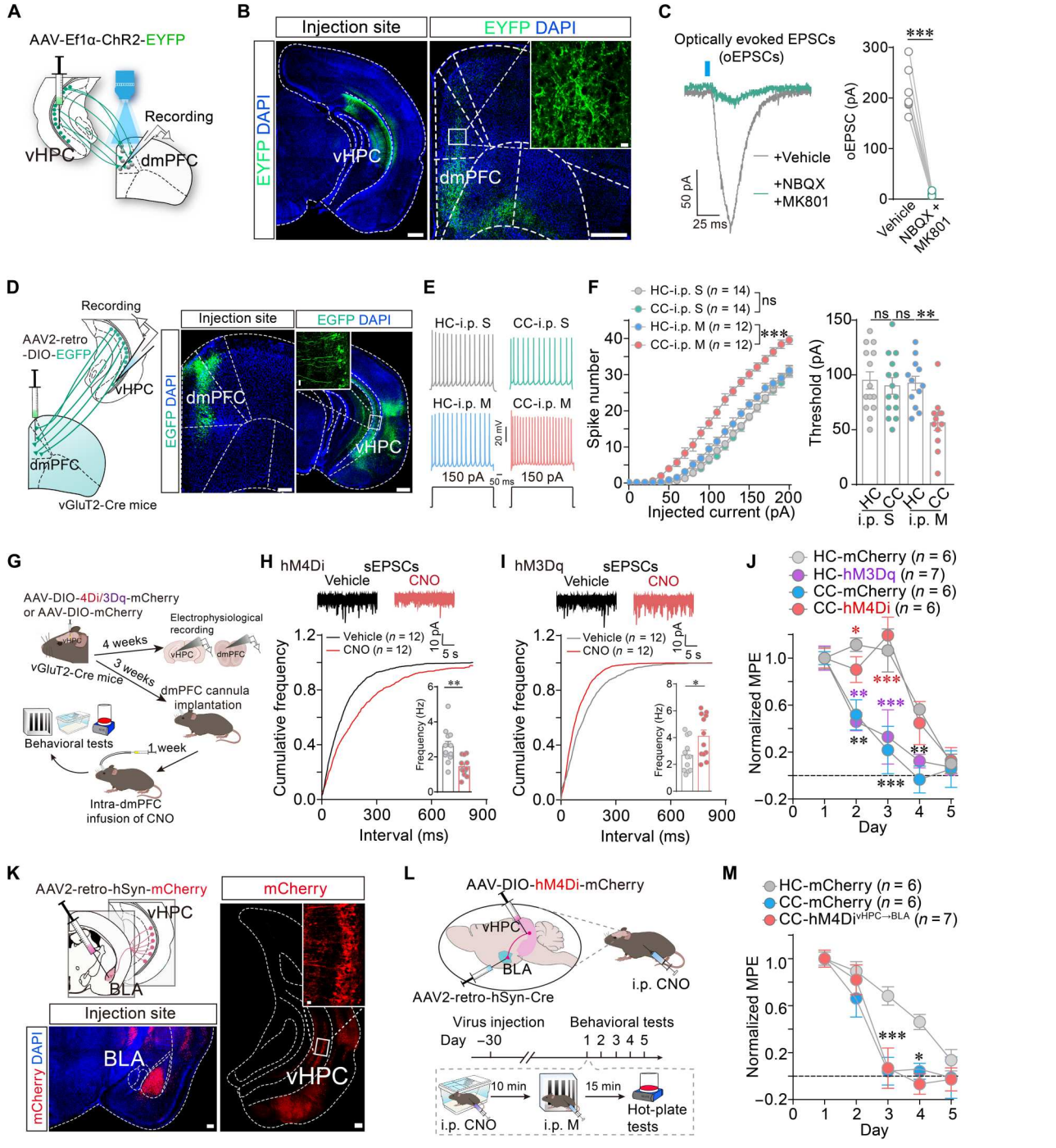

Fig. 3. Identification of the Glu$^{vHPC→dmPFC}$ pathway mediating AOAT. (**A**) Schematic of electrophysiological recording paradigm. (**B**) Representative images showing the virus injection site (left) and labeled axon terminals (right). Scale bars, 500 and 10 μm (inset). (**C**) Representative traces (left) and average amplitudes (right) of oEPSCs in dmPFC neurons before and after NBQX plus MK801 application. (**D**) Left: Schematic of electrophysiological recording of EGFP$^+$ Glu$^{vHPC→dmPFC}$ neurons. Right: Representative images showing the virus injection site and the retrograde-labeled neurons. Scale bars, 500 μm (dmPFC), 200 μm (vHPC), and 20 μm (inset). (**E** and **F**) AP spiking patterns (E) and spike numbers and thresholds (F) for AP firing of the Glu$^{vHPC→dmPFC}$ neurons of HC-mice and CC-mice receiving saline or morphine injection, respectively. (**G**) Schematic of chemogenetics. (**H** and **I**) Top: Representative trances of sEPSCs of the dmPFC neurons following bath application of ACSF and then CNO. Bottom: Cumulative fraction plots and quantification (inset) of sEPSC frequency. (**J**) Morphine analgesic tolerance in HC-mice and CC-mice with or without chemogenetic activation or inactivation of Glu$^{vHPC→dmPFC}$ terminals via bilateral intra-dmPFC injection of CNO (1 μg per mice). (**K**) Schematic showing retrograde tracing from BLA to vHPC and representative images showing the virus injection site in the BLA and retrograde-labeled neurons in vHPC. Scale bars, 200 and 10 μm (inset). The experiment was repeated in three mice with similar results. (**L**) Schematic of chemogenetics. (**M**) Morphine analgesic tolerance in the CC-mice with or without the chemogenetic inactivation of the BLA-projecting vHPC neurons and in the HC-mice. Data are presented as means ± SEM. *P < 0.05, **P < 0.01, and ***P < 0.001 by paired t test (C, H, and I) and one- and two-way ANOVA with Bonferroni post hoc test (F, J, and M); ns, not significant (P > 0.05).

analgesic effect induced by morphine (Fig. 3M and fig. S14), indicating that the vHPC→BLA projection is not involved in the mechanism of action for AOAT.

AOAT requires promotion of dmPFC inputs to BLA

We further explored the role of dmPFC→BLA circuitry in the development of AOAT based on our observations from c-Fos and neuronal ablation experiments. In line with previous studies (*51*–*53*), the projection from dmPFC neurons to BLA neurons was confirmed by retrograde viral tracing following microinjection of AAV2-retro-mCherry into BLA (Fig. 4A). We next used DREADDs approach to selectively manipulate the BLA-projecting dmPFC neurons (Fig. 4B). We injected AAV2-retro-Cre into BLA and AAV-DIO-hM4Di/hM3Dq-mCherry into dmPFC in an attempt to retroactively express hM4Di/hM3Dq-mCherry in the BLA-projecting dmPFC neurons (fig. S15, A and E). The functional expression of hM4Di/hM3Dq-mCherry in dmPFC was characterized by electrophysiological slice recording (fig. S15, B, C, F, and G). HM4Di-based chemogenetic inactivation of the BLA-projecting dmPFC neurons induced by CNO (1 mg/kg, intraperitoneally) suppressed the development of AOAT in CC-mice without significantly altering morphine-induced acute analgesic effect (Fig. 4C and fig. S15D). Conversely, hM3Dq-based chemogenetic activation of these BLA-projecting dmPFC neurons significantly accelerated the development of morphine analgesic tolerance (Fig. 4D) without affecting acute morphine analgesia in HC-mice (fig. S15H).

We next performed calcium imaging to examine in vivo neuronal activity during AOAT in the BLA-projecting dmPFC neurons in freely moving mice as previously described (*54*). Briefly, GCaMP6f, a genetically encoded Ca^{2+} indicator, was expressed in the BLA-projecting dmPFC neurons via intra-dmPFC injection of AAV-DIO-GCaMP6f and intra-BLA injection of AAV2-retro-Cre (Fig. 4E). A gradient refractive index lens was then implanted into the mouse dmPFC region to record transient Ca^{2+} events in individual neurons in the same field of view, while mice freely explored the morphine-conditioned context (Fig. 4, F and G, and movie S1).

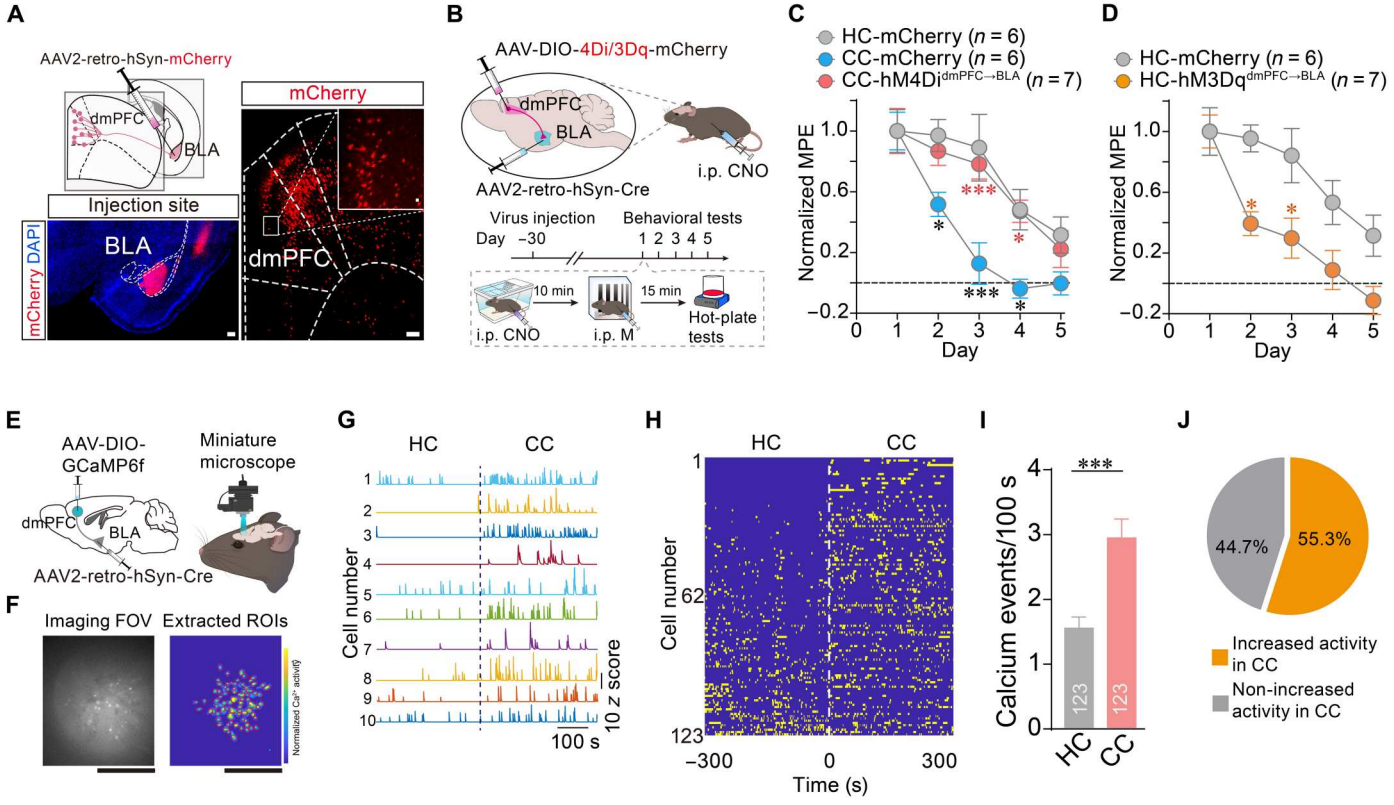

Fig. 4. Role of the BLA-projecting dmPFC neurons in AOAT. (**A**) Schematic showing retrograde tracing from BLA to dmPFC (upper left). Representative images showing the virus injection site in the BLA (lower left) and retrograde-labeled mCherry$^+$ neurons in dmPFC (right). Scale bars, 200 and 10 μm (inset). The experiment was repeated in three mice with similar results. (**B**) Schematic showing chemogenetic manipulation of the BLA-projecting dmPFC neurons. (**C**) Morphine analgesic tolerance in the CC-mice with or without chemogenetic inactivation of the BLA-projecting dmPFC neurons and in the HC-mice. (**D**) Morphine analgesic tolerance in the HC-mice with or without chemogenetic activation of the BLA-projecting dmPFC neurons. (**E**) Schematic showing the procedure for expressing GCaMP6f in the BLA-projecting dmPFC neurons and in vivo microendoscopic imaging of calcium signals in these neurons in freely moving mice. (**F**) Left: Example frame from a raw calcium imaging video. Right: Extracted region of interest (ROI) footprints superimposed on the maximum intensity projection. FOV, field of view. Scale bars, 100 μm. (**G**) Representative calcium signal traces of the BLA-projecting dmPFC neurons of mice during exploration of the HC and CC after AOAT training. (**H** and **I**) Heatmap of calcium responses (H) and frequency of calcium events (I) for all the recorded BLA-projecting dmPFC neurons when AOAT-trained mice were stationed in HC and CC (n = 123 neurons from three mice). (**J**) Proportions of the BLA-projecting dmPFC neurons with an increased or nonincreased frequency of calcium events when AOAT-trained mice were exploring CC as compared to HC. Data are presented as means ± SEM. *P < 0.05 and ***P < 0.001 by unpaired t test (I) or two-way ANOVA with Bonferroni post hoc test (C and D); ns, not significant (P > 0.05).

The BLA-projecting dmPFC neurons exhibited a significant increase in the frequency of calcium events in the AOAT-trained mice, when they were stationed in CC as compared to HC (Fig. 4, H and I). Nearly 55.3% (68 of 123) of the BLA-projecting dmPFC neurons in AOAT-trained mice exhibited significantly increased activity during CC exploration (Fig. 4J), suggesting that half of the dmPFC→BLA projections are involved in the development of AOAT. Notably, neither the context (CC) alone nor the HC associated with morphine usage could affect the neuronal activity of the BLA-projecting dmPFC neurons (fig. S16). Thus, these results indicate that the increase in BLA-projecting dmPFC neuronal activity is due to the context paired with morphine rather than the feature of context alone.

AOAT requires activation of $CCK^{dmPFC→BLA}$ neurons

Our discovery that dmPFC mediates AOAT motivated us to examine whether the dmPFC neurons express any distinct genes associated with opioids. To determine molecular targets in dmPFC that contribute to AOAT, we conducted RNA-sequencing (RNA-seq) analysis to examine the expression profiles of 16 common opioid-related genes in dmPFC. We observed a robust expression of *CCK* mRNA in dmPFC, although the *CCK* mRNA level was not changed during the development of morphine analgesic tolerance (Fig. 5A and fig. S17). CCK is a well-characterized anti-opioid peptide in the central nervous system (CNS) (*25*), and this peptide was found to play a role in the development of AOAT in an animal study (*16*). To verify the existence of the dmPFC CCKergic (CCK^{dmPFC}) neurons, we crossed a mouse line expressing Cre under the control of the *CCK* promoter (CCK-CreER) with Ai3 (a Cre-dependent EYFP reporter line) mice, and we detected a substantial population of CCK^+ neurons in dmPFC of CCK-CreER::Ai3 mice (Fig. 5B).

We next examined whether the BLA-projecting dmPFC neurons are also CCKergic by injecting AAV2-retro-DIO-EGFP into BLA of CCK-CreER mice (Fig. 5C). Retrograde tracing specifically revealed a large number of $EGFP^+$ neurons in dmPFC, but not in vHPC (Fig. 5C and fig. S18). The $EGFP^+$ signals were colocalized with CCK8s immunoreactivity in dmPFC (Fig. 5C). On the other hand, anterograde tracing revealed a CCKergic projection to BLA from dmPFC because a strong signal of CCK^{dmPFC} axon terminals was detected in BLA of the CCK-CreER mice receiving intra-dmPFC injection of AAV-DIO-EGFP (Fig. 5, D and E).

BLA has been found to have a cortex-like brain region composed mainly of glutamatergic neurons (*55*, *56*). Using primary antibodies to highlight CaMKII, a specific marker of glutamatergic neurons, we found that the $EGFP^+$ axon terminals from the CCK^{dmPFC} neurons were close to the $CaMKII^+$ neurons within BLA (Fig. 5F). We next used rabies virus (RV)–based retrograde monosynaptic tracing approach to determine the synaptic connection between the CCK^{dmPFC} neurons and the Glu^{BLA} neurons. Specifically, a mixture of Cre-dependent helper viruses (AAV-DIO-RVG to reinstate the trans-synaptic property of RV and AAV-DIO-TVA-GFP to facilitate selective infection) was injected into BLA of vGluT2-Cre mice. A modified RV (EnvA-pseudotyped RV-ΔG-DsRed) was injected into the same brain region 3 weeks after the helper virus injection (Fig. 5G). A large number of monosynaptic retrograde-labeled $DsRed^+$ neurons were observed in dmPFC and several other brain regions (Fig. 5H and fig. S19), and 79% of these neurons were CCK-immunopositive (Fig. 5I). Together, these results indicate that CCK^{dmPFC} neurons form direct synaptic contacts with Glu^{BLA} neurons.

Next, we investigated the in vivo impact of the $CCK^{dmPFC→BLA}$ projections on AOAT behavior. To examine whether these CCKergic projections are activated during AOAT, we first targeted the $CCK^{dmPFC→BLA}$ neurons by injecting AAV2-retro-DIO-EGFP into BLA of CCK-CreER mice (Fig. 5J). Whole-cell recordings of the dmPFC $EGFP^+$ neurons showed significantly enhanced intrinsic excitability, evidenced by an increase in AP firing rates and a reduction in current threshold (i.e., minimal injected current required to evoke AP), in CC-mice as compared to HC-mice (Fig. 5, K and L). To examine whether the enhanced intrinsic excitability requires vHPC input, we then injected AAV-CaMKII-hM4Di-mCherry into vHPC and AAV2-retro-DIO-EGFP into BLA of CCK-CreER mice (fig. S20A). After the full virus expression, these mice received CNO (1 mg/kg, intraperitoneally) injections followed by morphine treatments in CC each day for three consecutive days. The chemogenetic inhibition of Glu^{vHPC} neurons significantly suppressed the increased intrinsic excitability of the $EGFP^+$ $CCK^{dmPFC→BLA}$ neurons (fig. S20, B to D).

We next performed chemogenetic manipulation of the $CCK^{dmPFC→BLA}$ projection in CCK-CreER mice after intra-dmPFC injection of AAV-DIO-hM4Di-mCherry, AAV-DIO-hM3Dq-mCherry, or AAV-DIO-mCherry (Fig. 5M). The physical and functional expression of hM4Di/hM3Dq-mCherry in dmPFC was confirmed by both histological mapping and electrophysiological slice recording (fig. S21, A, B, K, and L). Chemogenetic inhibition of the $hM4Di^+$ $CCK^{dmPFC→BLA}$ terminals selectively inhibited AOAT development in the CC-mice without significantly altering acute analgesic effects of morphine (Fig. 5N and fig. S21C). This chemogenetic inhibition of the $hM4Di^+$ $CCK^{dmPFC→BLA}$ terminals did not affect the development of morphine analgesic tolerance and acute morphine analgesia in the HC-mice (fig. S21, D to F). To further examine the role of this pathway in AOAT, we transferred the mice to a novel environment (NE) on day 5 after 4-day morphine injections in HC or CC (fig. S21, G and I). On day 5, for the HC-mice, morphine was ineffective in both HC and NE. For the CC-mice, morphine became effective in NE, but not in CC, and chemogenetic inhibition of the $CCK^{dmPFC→BLA}$ terminals significantly inhibited morphine tolerance in CC, but not in NE (fig. S21, H and J), indicating that the CC, but not the HC, serves as an associative context. Furthermore, chemogenetic activation of the $hM3Dq^+$ $CCK^{dmPFC→BLA}$ terminals significantly exacerbated the development of morphine analgesic tolerance in the HC-mice without affecting the acute analgesic effects of morphine and basal pain threshold (Fig. 5O and fig. S21, M and N). These findings indicate that activation of the $CCK^{dmPFC→BLA}$ projection is essential for the development of AOAT.

In view of the critical role of the CCK^{dmPFC} neurons in the development of AOAT, we further characterized the connectivity of the Glu^{vHPC} neurons and CCK^{dmPFC} neurons using an RV-mediated retrograde trans-monosynaptic tracing system (Fig. 6A). The monosynaptic input neurons were detected in vHPC, and 71.9% of these neurons were CaMKII immunopositive (Fig. 6, B and C), supporting the idea that the CCK^{dmPFC} neurons receive monosynaptic projections from the Glu^{vHPC} neurons.

Next, to assess the functional tandem synaptic connectivity of the $Glu^{vHPC}→CCK^{dmPFC}→Glu^{BLA}$ pathway, we infected vHPC with AAV-ChR2-EYFP and BLA with AAV2-retro-DIO-mCherry

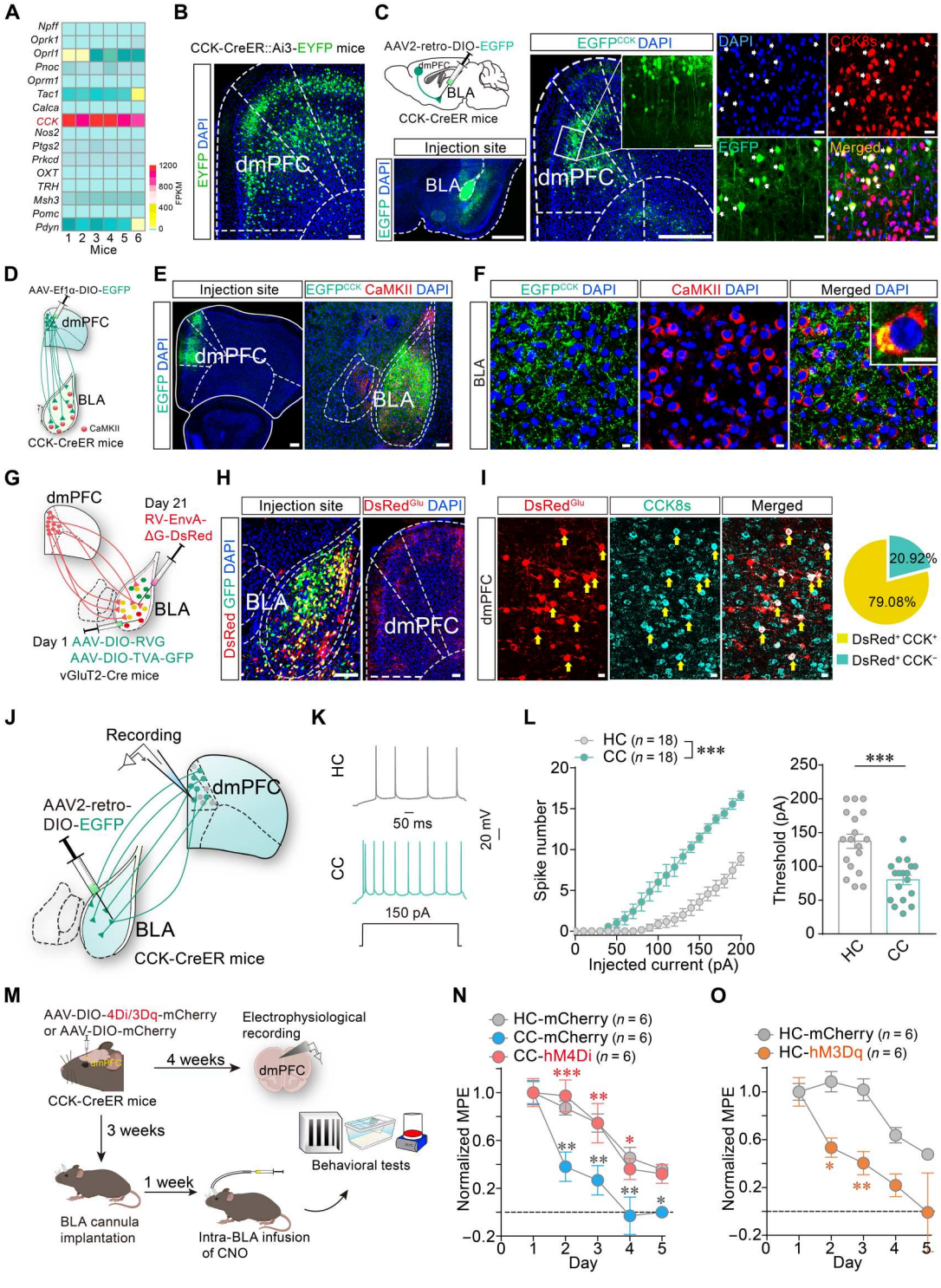

Fig. 5. Identification of the CCK$^{dmPFC\rightarrow Glu^{BLA}}$ pathway mediating AOAT. (**A**) Heatmap of RNA-seq data for 16 opioid-related genes; data are reported in FPKM (fragments per kilobase million). (**B**) Representative image showing EYFP$^+$ neurons in dmPFC of CCK-CreER::Ai3-EYFP reporter mice. Scale bar, 100 μm. (**C**) Schematic of AAV2-retro virus injection in CCK-CreER mice (upper left) and representative images of viral expression in the indicated nuclei (lower left and middle). Scale bars, 500 and 100 μm (inset). EGFP$^+$ neurons co-localized with CCK8s immunoreactivity in dmPFC (right). Scale bars, 20 μm. (**D**) Schematic of AAV-Ef1a-DIO-EGFP injection in CCK-CreER mice. (**E** and **F**) Representative images showing AAV-Ef1a-DIO-EGFP infection in dmPFC (E, left) and the EGFP$^+$ axon terminals that intermingled with CaMKII$^+$ neurons in BLA (E, right, and F). Scale bars, 100 μm (E) and 10 μm (F). (**G**) Schematic of the procedure for tracing of Cre-dependent retrograde trans-monosynaptic RV. (**H**) Representative images showing starter cells in the BLA and DsRed$^+$ neurons in dmPFC. Scale bars, 100 μm. (**I**) Representative images (left) and percentage analysis (right) of DsRed$^+$ neurons that expressed CCK8s in dmPFC (n = 1372 neurons from three mice). (**J**) Schematic of electrophysiological recording of EGFP$^+$ CCK$^{dmPFC\rightarrow BLA}$ neurons. (**K** and **L**) AP spiking patterns (K) and spike numbers and thresholds (L) for AP firing of the CCK$^{dmPFC\rightarrow BLA}$ neurons of HC-mice and CC-mice. (**M**) Schematic of chemogenetics. (**N** and **O**) Morphine analgesic tolerance in CC-mice (N) and HC-mice (O) with or without chemogenetic activation or inactivation of the CCK$^{dmPFC\rightarrow BLA}$ terminals. Morphological analyses (B, C, E, H, and I) were independently repeated with similar results in four mice. Data are presented as means ± SEM. *P < 0.05, **P < 0.01, and ***P < 0.001 by unpaired t test (L, right) and two-way ANOVA with Bonferroni post hoc test [L (left), N, and O].

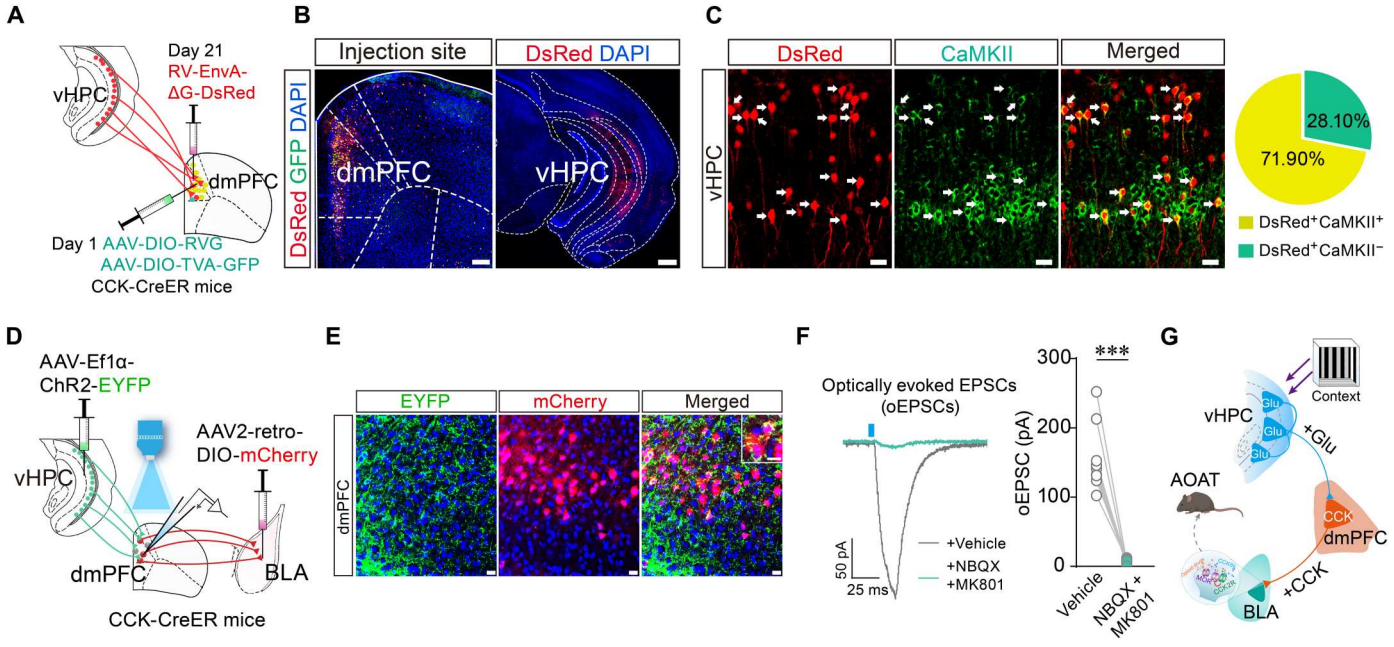

Fig. 6. Identification of the Glu^{vHPC}→CCK^{dmPFC}→Glu^{BLA} pathway. (**A**) Schematic showing the procedure for retrograde tracing of the Glu^{vHPC}→CCK^{dmPFC} neurons using the Cre-dependent retrograde trans-monosynaptic RV. (**B**) Left: Representative image showing starter cells (yellow) coexpressing AAV-DIO-TVA-GFP (green), AAV-DIO-RVG, and RV-EnvA-ΔG-DsRed (red) in dmPFC of CCK-CreER mice. Scale bar, 200 μm. Right: Representative image showing DsRed$^+$ neurons in the vHPC retrograde traced from CCK^{dmPFC} neurons. Scale bar, 500 μm. (**C**) Left: Representative images showing DsRed$^+$ neurons that colocalized with CaMKII immunoreactivity in vHPC (white arrowheads). Scale bars, 10 μm. Right: Percentage of DsRed$^+$ neurons that coexpressed CaMKII in vHPC (n = 3704 neurons from five mice). (**D**) Schematic of the procedure for verification of the Glu^{vHPC}→CCK^{dmPFC}→Glu^{BLA} neuronal pathway using optogenetic methods combined with virus-mediated retrograde monosynaptic tracing. Whole-cell patch clamp recordings of the mCherry$^+$ neurons in BLA slices were conducted with laser stimulation. (**E**) Representative images showing EYFP$^+$ axon terminals of vHPC neurons that intermingled with mCherry$^+$ CCK$^{dmPFC→BLA}$ neurons in dmPFC. Scale bars, 20 and 5 μm (inset). (**F**) Representative traces (left) and average amplitudes (right) of oEPSCs in the mCherry$^+$ CCK$^{dmPFC→BLA}$ neurons. (**G**) Working model of the hierarchical Glu^{vHPC}→CCK^{dmPFC}→Glu^{BLA} neuronal pathway that mediates AOAT. Morphological analyses (B, C, and E) were independently repeated with similar results in three mice. Data are presented as means ± SEM. ***P < 0.001 by paired t test.

in CCK-CreER mice. These viral injections should allow us to specifically label the CCK$^{dmPFC→BLA}$ neurons and to record the responses of the infected neurons to optogenetic activation of the vHPC axon terminals in dmPFC brain slices (Fig. 6, D and E). Photostimulation of vHPC fibers in dmPFC elicited robust oEPSCs in the mCherry$^+$ CCK$^{dmPFC→BLA}$ neurons. These oEPSCs were significantly blocked by bath application of NBQX and MK801 (Fig. 6F). These observations add further evidence suggesting a Glu^{vHPC}→CCK^{dmPFC}→Glu^{BLA} neuronal pathway responsible for AOAT (Fig. 6G).

CCK2 receptors in BLA mediate AOAT through MOR inhibition

The data presented above suggest that BLA neurons are the downstream target of AOAT signaling pathway. It is widely accepted that there are three major types of opioid receptors—the MOR, the δ-opioid receptor (DOR), and the κ-opioid receptor (KOR), which are involved in opioid analgesia in the CNS (*43*). We performed the following experiments to determine which subtype of opioid receptors in BLA could mediate morphine analgesia (Fig. 7A). Intra-BLA injection of nonselective antagonist naloxone and selective MOR antagonist CTOP both dose-dependently inhibited the analgesic effect of systemic morphine (Fig. 7, B and C) without altering the basal pain threshold (fig. S22). In contrast, morphine analgesia was not altered in mice receiving intra-BLA injection of DOR antagonist naltrindole or KOR antagonist norbinaltorphimine (nor-BNI) (Fig. 7, D and E). To further validate the role of BLA MORs in acute morphine analgesia and morphine analgesic tolerance, we specifically knocked out the MORs in BLA using *Oprm1*$^{fl/fl}$ mice (*57*) with bilateral intra-BLA injection of AAV-Cre-EGFP (Fig. 7F). Immunohistochemistry and quantitative reverse transcription polymerase chain reaction (qRT-PCR) analysis confirmed the efficiency of the conditional knockout (fig. S23, A and B). Depletion of MOR from BLA neurons significantly suppressed the analgesic effect of systemic morphine (Fig. 7F), accelerated the development of morphine analgesic tolerance in the HC-mice, and slightly enhanced the AOAT development in the CC-mice (fig. S23, C and D).

To further investigate whether the BLA MOR is involved in AOAT, we injected DAMGO, an MOR-selective agonist, into BLA of mice 4 days after repeated morphine treatments (Fig. 7, G and H). On day 5, we observed that intra-BLA administration of DAMGO induced remarkable analgesic effects in the naïve mice and weak antinociception in the HC-mice. However, this DAMGO-induced analgesic effect was completely lost in the CC-mice (Fig. 7I). These results suggest that BLA MORs mediate a direct opioid analgesia, and the further dysfunction of the BLA MORs caused by context-associated morphine may act as a downstream effect of activation of the neuronal circuit underlying AOAT.

There are two main subtypes of CCK receptors, CCK1R and CCK2R (*58*). In view of the structural evidence of the CCK$^{dmPFC→BLA}$ projections, we asked which type of CCK receptors

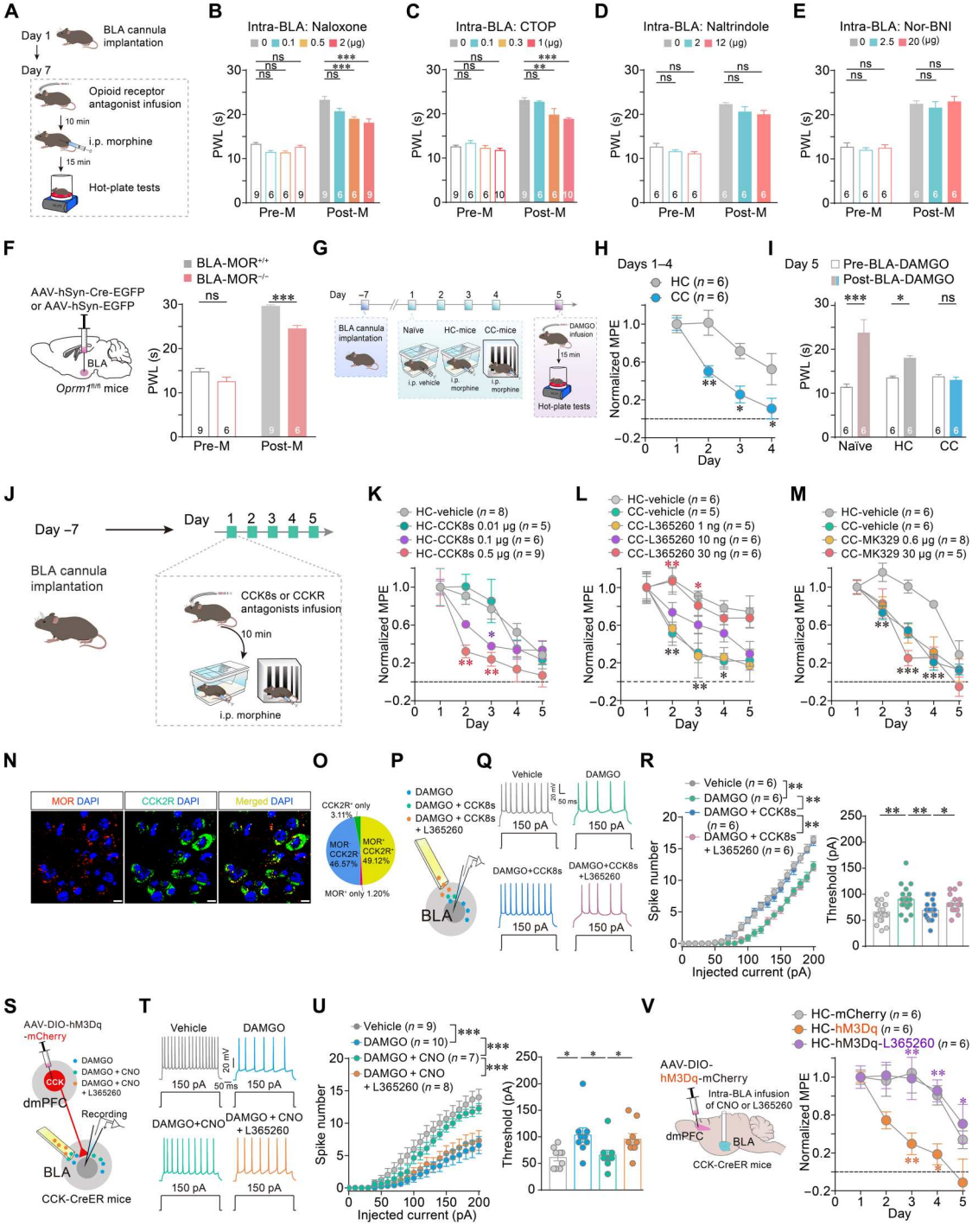

Fig. 7. Identification of specific subtypes of CCK receptors and opioid receptors in BLA involved in AOAT. (**A**) Schematic of BLA infusion of opioid receptor antagonists. (**B** to **E**) Quantitative PWL of mice before (pre-M) and after (post-M) morphine (5 mg/kg, intraperitoneally) injection with intra-BLA infusion of naloxone (B), CTOP (C), naltrindole (D), or nor-BNI (E) at various doses. (**F**) Left: Schematic of AAV-Cre injection in *Oprm1*$^{fl/fl}$ mice. Right: Quantitative PWL of *Oprm1*$^{fl/fl}$ mice with (BLA-MOR$^{-/-}$) or without (BLA-MOR$^{+/+}$) knockout of BLA MORs. (**G**) Schematic of 4-day AOAT development and intra-BLA infusion of DAMGO on day 5. (**H**) Morphine analgesic tolerance in HC-mice and CC-mice. (**I**) Quantitative PWL of mice before and after intra-BLA infusion of DAMGO (100 ng per mice) on day 5. (**J**) Schematic of BLA infusion of CCK receptor agonists or antagonists. (**K** to **M**) Dose-dependent effects of intra-BLA injection of CCK8s (K), L365260 (L), and MK329 (M) on the development of morphine analgesic tolerance. (**N** and **O**) Representative images (N) and percentage analysis (O) of MOR^{+} neurons and CCK2R^{+} neurons in BLA. The experiment was repeated with similar results in five mice. Scale bars, 10 μm. (**P** to **U**) Schematic of electrophysiological recording paradigm (P and S). AP spiking patterns (Q and T) and spike numbers and thresholds (R and U) for AP firing of the BLA neurons of C57BL/6J mice (P to R) and CCK-CreER mice (S to U). (**V**) Left: Schematic of chemogenetics. Right: Morphine analgesic tolerance in HC-mice with or without chemogenetic activation of the CCK$^{dmPFC\rightarrow BLA}$ terminals and the effect of L365260 (30 ng per mice). Data are presented as means ± SEM. *P < 0.05, **P < 0.01, and ***P < 0.001 by one- and two-way ANOVA with Bonferroni post hoc test; ns, not significant (P > 0.05).

in BLA mediates AOAT. To answer this question, we performed pharmacological experiments using intra-BLA injection of CCK receptor agonists and antagonists (Fig. 7J). Intra-BLA infusion of sulfated CCK octapeptide (CCK8s), a major form of endogenous CCK in the CNS (*59*), significantly accelerated the development of morphine tolerance in a dose-dependent manner (Fig. 7K). CCK8s did not significantly alter the basal pain threshold (fig. S24, A and B). Both systemic and intra-BLA infusion of L365260, a specific CCK2R antagonist, dose-dependently suppressed the development of AOAT (Fig. 7L and fig. S24C) without altering the acute analgesic effect of morphine, the basal pain threshold, and the nonassociative morphine analgesic tolerance (fig. S24, D to H). However, intra-BLA injection of the CCK1R antagonist MK329 failed to affect AOAT and acute morphine analgesia (Fig. 7M and fig. S24I). These results indicate the dominant role of CCK2R in mediating the effect of exogenous or endogenous CCK in BLA.

Furthermore, double-labeling immunofluorescence experiments showed that 49.12% of BLA cells coexpressed CCK2Rs and MORs, indicating a possibility of a CCK2R-MOR interaction (Fig. 7, N and O). Whole-cell patch clamp recordings of BLA brain slices demonstrated that bath application of DAMGO significantly decreased the rate of AP firing in BLA neurons. This decrease was completely blocked by addition of CCK8s, and this inhibitory effect induced by CCK8s was also prevented by L365260 (Fig. 7, P to R).

Next, we performed electrophysiological experiments to examine whether the endogenous CCK released from the $CCK^{dmPFC\rightarrow BLA}$ terminals could antagonize the function of opioids in BLA. For this purpose, we infected the CCK^{dmPFC} neurons in CCK-CreER mice with AAV-DIO-hM3Dq-mCherry and then conducted whole-cell patch-clamp recordings in BLA brain slices (Fig. 7S). Bath application of DAMGO markedly reduced the excitability of BLA neurons, which was restored by the CNO-induced chemogenetic activation of the $CCK^{dmPFC\rightarrow BLA}$ terminals. The effect of CNO was significantly suppressed by bath application of L365260 (Fig. 7, T and U), suggesting an endogenous CCK-mediated effect. Furthermore, intra-BLA injection of L365260 significantly blocked the exacerbation of morphine analgesic tolerance caused by the chemogenetic activation of the $CCK^{dmPFC\rightarrow BLA}$ terminals in HC-mice (Fig. 7V and fig. S24J). Together, all these results demonstrate that endogenous CCK released from dmPFC neurons may mediate AOAT by activating CCK2Rs and subsequently antagonizing MORs in BLA neurons.

DISCUSSION

We have used a series of viral tracing and chemo/optogenetic strategies in vitro and in vivo to identify a neuronal circuit in the brain specialized for the control of AOAT. Activation of this circuit by drug-associated context selectively accelerates the development of tolerance of the analgesic effect of morphine and fentanyl. Clinically, the analgesic treatment for chronic pain starts from low-dose opioid agonists (*60*–*62*). Several physiological and pathological processes are involved in the development of analgesic tolerance induced by opioid drugs, especially low-dose opioids. In the present study, we observed that AOAT did occur when a low-to-moderate dose range of morphine was used in treating acute pain, chronic inflammatory pain, and neuropathic pain and even in causing side effects such as respiratory depression. However, the $Glu^{vHPC\rightarrow dmPFC}$ pathway specifically mediates the context-associated tolerance on opioid analgesic effects to various forms of pain, but not the tolerance to other opioid effects such as the respiratory depression. This is a fantastic characteristic since intervention in this circuit will enhance the opioid analgesic effects during repeated opioid use in the same clinical setting and mitigate the respiratory suppressive effects of opioids by maintaining its tolerance. This suggests that the AOAT circuit may serve as a potential target to treat analgesic tolerance at the early stage of the therapy using opioid agonists.

Numerous studies have indicated that dmPFC, vHPC, and their connections are crucial for context-associated behaviors (*63*). For instance, inactivation of dmPFC by the sodium channel blocker tetrodotoxin decreases the expression of contextual fear (*64*). Another study using calcium imaging and optogenetic methods showed that vHPC neurons respond to anxiety-associated contexts, and that inactivation of these vHPC neurons reduces avoidance of anxiogenic environments (*65*). Functional connectivity studies have demonstrated that environmental information is sent from the hippocampus to dmPFC in rats during spatial context-guided memory tasks (*63*, *66*). Consistently, this study has revealed a hierarchical organization by which the brain regions including vHPC, dmPFC, and BLA mediate AOAT, a clinical typical context-conditioned behavior, but has not been given sufficient attention. This hypothesis is based on the following observations. While distinguishable expression of c-Fos was observed in all three areas of vHPC, dmPFC, and BLA during the development of AOAT, only ablation of vHPC inhibited both AOAT and enhancement of c-Fos signal in dmPFC and BLA neurons. Ablation of BLA neurons directly disrupted opioid analgesia as expected but did not affect the context-induced enhancement of c-Fos signal in dmPFC and BLA neurons. This suggests that AOAT develops via hierarchical pathway starting from enhancement of vHPC neuronal activity and taking BLA as the downstream output. We further dissected subpopulation of neurons and molecular components involved in AOAT in the descending projections from vHPC to dmPFC and downstream BLA using retrograde/anterograde tracing and chemogenetic/optogenetic manipulation. We observed that AOAT promoted the activity of $Glu^{vHPC\text{-}dmPFC}$ projection. We also identified a pathway of $CCK^{dmPFC\text{-}BLA}$ projection that disrupted MOR function by activation of CCK2Rs on Glu^{BLA} neurons.

Emerging evidence suggests that opioid system plays a crucial role in context- and cognition-associated behaviors (*67*). For instance, placebo analgesia, one of the most striking cases of cognitive and contextual modulation of pain perception, can be antagonized by the nonselective opioid receptor antagonist naloxone (*68*). Although the context- and cognition-associated opioid tolerance has been well established (*16*, *18*, *69*), the underlying neurological mechanism is still at large. Consistent with previous observations (*70*–*72*), we find that BLA is a critical locus for mediating morphine analgesia, since antagonism and genetic ablation of MORs in BLA significantly suppressed the analgesic effects of systemic morphine. Thus, endogenous CCK in BLA, released from the $CCK^{dmPFC\rightarrow BLA}$ terminals, is a major factor enhancing opioid tolerance, possibly due to the high-efficiency anti-opioid characteristics of CCK (*25*, *38*, *73*). It should be mentioned that although we demonstrate that the $CCK^{dmPFC\rightarrow BLA}$ neurons specifically mediate AOAT by releasing CCK, these neurons may also coexpress glutamate, γ-aminobutyric acid (GABA), or other neurotransmitters (*74*, *75*). Whether

the coexpressed neurotransmitters can also modulate AOAT remains unknown and requires further investigation.

Our results establish a Glu^{vHPC}→CCK^{dmPFC}→Glu^{BLA} circuitry mechanism specific to the development of tolerance to the analgesic effect of opioids. This neuronal ensemble orchestrates BLA MOR activity, rendering them a dynamic control of opioid analgesic tolerance. The decisive elements of this pathway are promising targets for therapeutic strategies to intervene in the development of tolerance to the opioid analgesia at the early stage.

MATERIALS AND METHODS

Mice

All procedures and husbandry conditions followed the standard animal care. Biosafety guidelines were approved by the Institutional Animal Use and Care Committee of the University of Science and Technology of China (agreement number: USCTACUC1901009). C57BL/6J, CCK-CreER [STOCK *Cck*$^{tm2.1\ (cre/ERT2)\ Zjh}$/J], Ai3 [B6.Cg-*Gt (ROSA) 26Sor*$^{tm3\ (CAG-EYFP)\ Hze}$/J], vGluT2-ires-Cre [STOCK *Slc17a6*$^{tm2\ (cre)\ Lowl}$/J, referred to as vGluT2-Cre], and *Oprm1*$^{fl/fl}$ mice were used for experiments. *Oprm1*$^{fl/fl}$ mice, allowing for conditional deletion of MORs in neurons with Cre recombinase by using the Cre/loxP strategy, were obtained from Y. Sun (Institute of Neuroscience, Chinese Academy of Sciences). All mice were group-housed with three to five per cage unless a cannula was implanted. All mice were maintained at 18° to 23°C with 40 to 60% humidity in a 12-hour light/12-hour dark cycle with ad libitum access to food and water. All behavioral experiments were performed on adult male or female mice (8 to 12 weeks old).

Stereotaxic injection and cannula implantation

Mice were deeply anesthetized with an intraperitoneal injection of pentobarbital sodium (80 mg/kg) and then fixed on a stereotactic frame (RWD Life Science, Shenzhen, China). Chlortetracycline hydrochloride (Beijing Shuangji Pharmaceutical Co. Ltd) was applied to keep the eyes moist. An incision along the brain raphe was made to expose the skull, and then a stereotaxic drill was used to perforate at the target brain area. Virus injections were applied through a glass micropipette fixed on a microsyringe pump (Legato 130, KD Scientific) at a rate of 60 nl/min. The micropipette was slowly pulled out 10 min after virus infusion to allow diffusion of the virus.

For brain cannula implantation, two guide cannulas (RWD Life Science, Shenzhen, China) were bilaterally implanted above the nuclei (BLA, vHPC, or dmPFC). For lateral ventricle (LV) cannula implantation, a guide cannula was unilaterally implanted into the LV. The cannula was stabilized to the skull with dental cement, and a cap was inserted into each cannula to prevent blockage. The animals were allowed to recuperate for at least one week before behavioral experiments. Cannula placements were verified by injection of Nissl dye after behavioral experiments. The data from mice with inaccurate cannula placement were discarded.

The stereotaxic coordinates, defined as anterior-posterior (AP) and medial-lateral (ML) from bregma and dorsal-ventral (DV) on the brain surface at target coordinate, were as follows: LV (AP, −0.20 mm; ML, +1.00 mm; DV, −2.00 mm), dmPFC (AP, +2.34 mm; ML, ±0.20 mm; DV, −0.85 mm), BLA (AP, −1.20 mm; ML, ±3.20 mm; DV, −4.54 mm), vHPC (AP, −3.16 mm; ML, ±3.50 mm; DV, −3.80 mm and AP, −3.16 mm; ML, ±2.75 mm; DV, −2.44 mm). The coordinates would be adjusted appropriately according to the weight and age of mice and verified in several mice that were initially operated on.

Virus injections

Neuronal ablation

For dmPFC, BLA, and vHPC neuron ablation, AAV2/9-Ef1α-flex-taCasp3-TEVp (titer: 1.15×10^{13} genome copies/ml) and AAV2/9-hSyn-Cre (titer: 2.25×10^{12} genome copies/ml) were bilaterally coinjected (1:1) into dmPFC (400 nl per side), BLA (400 nl per side), or vHPC (600 nl per side) of C57BL/6J mice. AAV2/9-Ef1α-DIO-EGFP (titer: 5.26×10^{12} genome copies/ml) was used as a control. Behavioral testing was performed four weeks after virus injection.

MOR conditional knockout

For conditional deletion of MORs in BLA neurons, AAV2/9-hSyn-Cre-EGFP (titer: 3.21×10^{12} genome copies/ml, 400 nl per side) was bilaterally injected into BLA of the *Oprm1*$^{fl/fl}$ mice. AAV2/9-hSyn-EGFP (titer: 2.05×10^{12} genome copies/ml, 400 nl per side) was used as a control. Behavioral testing and immunohistochemistry experiments were performed four weeks after virus injection.

Neuronal tracing

For retrograde tracing, AAV2/2-retro-hSyn-mCherry (titer: 5.27×10^{12} genome copies/ml, 300 nl per side) was unilaterally injected into BLA of C57BL/6J mice to label neurons projecting to BLA. AAV2/2-retro-Ef1α-DIO-EGFP (titer: 5.26×10^{12} genome copies/ml, 300 nl per side) was unilaterally injected into BLA of CCK-CreER mice to label the BLA-projecting CCKergic neurons or unilaterally injected into dmPFC of vGluT2-Cre mice to label the dmPFC-projecting glutamatergic neurons. Four weeks later, expression of mCherry or EGFP was examined in the whole brain, or electrophysiological experiments were performed.

For retrograde monosynaptic tracing, helper viruses including AAV2/9-Ef1α-DIO-RVG (titer: 2.25×10^{11} genome copies/ml) and AAV2/9-Ef1α-DIO-TVA-GFP (titer: 2.78×10^{11} genome copies/ml) were unilaterally coinjected (1:1 ratio in 350 nl) into BLA of vGluT2-Cre mice or dmPFC of CCK-CreER mice. Three weeks later, the ΔG-RV that encoded DsRed (RV-EnvA-ΔG-DsRed, titer: 4.50×10^{6} genome copies/ml, 200 nl per side) was unilaterally injected into the same brain region. Ten days after the last injection, the mice were perfused and the brain slices were collected for detecting the DsRed signals and immunostaining with CCK8s- or CaMKII-specific antibodies.

For anterograde tracing, AAV2/9-Ef1α-DIO-EGFP (titer: 5.26×10^{12} genome copies/ml, 300 nl per side) was unilaterally injected into dmPFC of CCK-CreER mice. Four weeks later, the mice were perfused and the brain was sectioned for confocal imaging.

Neuronal circuit manipulation

For chemogenetically inactivating the dmPFC→BLA or vHPC→BLA projection, AAV2/2-retro-hSyn-Cre (titer: 5.51×10^{12} genome copies/ml, 400 nl per side) was bilaterally injected into BLA of C57BL/6J mice, and AAV2/9-Ef1α-DIO-hM4Di-mCherry (titer: 5.55×10^{12} genome copies/ml) was bilaterally injected into dmPFC (400 nl per side) or vHPC (600 nl per side). For chemogenetically activating the dmPFC→BLA projection, AAV2/2-retro-hSyn-Cre (titer: 5.51×10^{12} genome copies/ml, 400 nl per side) was bilaterally injected into BLA of C57BL/6J mice, and AAV2/9-Ef1α-DIO-hM3Dq-mCherry (titer: 2.70×10^{12} genome copies/ml, 400 nl per side) was bilaterally injected into dmPFC. Four weeks later, mice received daily CNO (1 mg/kg,

intraperitoneally) injection in the HC 10 min before morphine injection (5 mg/kg, intraperitoneally) during the AOAT training.

For chemogenetic manipulation of the $CCK^{dmPFC→BLA}$ projection, AAV2/9-Ef1α-DIO-hM3Dq-mCherry (titer: 2.70×10^{12} genome copies/ml, 400 nl per side) or AAV2/9-Ef1α-DIO-hM4Di-mCherry (titer: 5.55×10^{12} genome copies/ml, 400 nl per side) was bilaterally injected into dmPFC of CCK-CreER mice. For chemogenetic manipulation of the $Glu^{vHPC→dmPFC}$ projection, AAV2/9-Ef1α-DIO-hM3Dq-mCherry (titer: 2.70×10^{12} genome copies/ml, 600 nl per side) or AAV2/9-Ef1α-DIO-hM4Di-mCherry (titer: 5.55×10^{12} genome copies/ml, 600 nl per side) was bilaterally injected into vHPC of vGluT2-Cre mice. Guide cannulas for CNO administration were bilaterally implanted above BLA or dmPFC three weeks after virus injection. After one-week recovery, CNO (1 μg/μl, 0.5 μl per side) was daily microinjected into the bilateral BLA or dmPFC 10 min before morphine injection (5 mg/kg, intraperitoneally) in the HC, and the behavioral experiments were performed 15 min after morphine injection.

For optogenetic activation of the vHPC→dmPFC projection, AAV2/9-Ef1α-hChR2 (H134R)-EYFP (titer: 2.00×10^{12} genome copies/ml, 400 nl per side) was unilaterally injected into vHPC of C57BL/6J mice. Four weeks later, the electrophysiological recordings were performed.

For assessing the nature of the $Glu^{vHPC}→CCK^{dmPFC}→Glu^{BLA}$ pathway, AAV2/2-retro-Ef1α-DIO-mCherry (titer: 5.18×10^{12} genome copies/ml, 300 nl per side) was unilaterally injected into BLA of CCK-CreER mice, which had already received intra-vHPC injection of AAV2/9-Ef1α-hChR2 (H134R)-EYFP (titer: 2.00×10^{12} genome copies/ml, 600 nl per side). Four weeks later, the electrophysiological recordings were performed.

For assessing the role of vHPC input in the increased excitability in $CCK^{dmPFC→BLA}$ neurons during AOAT development, AAV2/2-retro-Ef1α-DIO-EGFP (titer: 5.26×10^{12} genome copies/ml, 300 nl per side) was unilaterally injected into BLA of CCK-CreER mice, which had already received intra-vHPC injection of AAV2/9-CaMKII-hM4Di-mCherry (titer: 5.0×10^{12} genome copies/ml, 600 nl per side). Four weeks later, the behavioral experiments and electrophysiological recordings were performed.

Injection sites of the virus were confirmed by observing the sites with fluorescence optics. The data from mice with inaccurate injection sites were discarded. The above viruses were purchased from BrainVTA, Wuhan, China.

Brain slice electrophysiological recording

Brain slice preparation

Mice were anesthetized with an intraperitoneal injection of pentobarbital sodium (80 mg/kg). After deep anesthesia, the mice were transcardially perfused by the ice-cold cutting solution with oxygen saturated (95% O_2/5% CO_2, pH 7.4, 300 to 310 mOsm), containing 30 mM NaCl, 26 mM $NaHCO_3$, 10 mM glucose, 194 mM sucrose, 4.5 mM KCl, 1.2 mM NaH_2PO_4, and 1 mM $MgCl_2$. The whole process of perfusion lasted approximately 2 min, with a total volume of 10 to 20 ml. After perfusion, the mouse coronal brain slices (300 μm) were collected using the vibrating microtome (Leica VT1200S) in ice-cold cutting solution with oxygen saturation. The brain slices were then transferred into the carbonated artificial cerebrospinal fluid (ACSF) containing 124 mM NaCl, 4.5 mM KCl, 1 mM $MgCl_2$, 2 mM $CaCl_2$, 1.2 mM NaH_2PO_4, and 26 mM $NaHCO_3$ (95% O_2/5% CO_2, pH 7.4, 300 to 310 mOsm) and incubated for at least 30 min at 32°C. After incubation with ACSF at room temperature for another 30 min, slices were transferred into a recording chamber and were continuously perfused with oxygenated ACSF. Recordings were performed using glass pipettes (5 to 8 megohms) filled with internal solution containing 145 mM K-gluconate, 4 mM $MgCl_2$, 10 mM EGTA, 5 mM Hepes, 0.2 mM Na–guanosine triphosphate (GTP), and 5 mM Mg–adenosine 5′-triphosphate (pH 7.2, ~280 mOsm). Neurons in the target area were visualized by infrared–differential interference contrast camera and fluorescent microscope (BX51WI, Olympus). MultiClamp 700B amplifier (Molecular Devices, Sunnyvale, CA) was used to amplify recorded signals. Digidata 1550A (National Instruments) was used to digitize analog signals at 3 kHz. Data analysis was performed by pClamp 10.4 software (Molecular Devices, Sunnyvale, CA).

AP recording

A step current (0 to 200 pA with 10-pA increment) was injected to trigger AP in a current-clamp mode after whole-cell configuration. To assess the $CCK^{dmPFC→BLA}$ and $Glu^{vHPC→dmPFC}$ neuronal intrinsic excitability, AAV2/2-retro-Ef1α-DIO-EGFP (titer: 5.26×10^{12} genome copies/ml, 300 nl per side) was unilaterally injected into BLA of CCK-CreER mice or dmPFC of vGluT2-Cre mice. Four weeks after virus injection, the mice were injected with morphine (5 mg/kg, intraperitoneally) or saline in HC or CC for 3 days. Then, brain slices were obtained 30 min after the last injection and electrophysiological recordings were performed on visually identified $EGFP^+$ neurons in dmPFC or vHPC under a fluorescent microscope. To verify the function of chemogenetic virus, electrophysiological recordings were performed on visually identified $mCherry^+$ neurons in the injection site with a fluorescent microscope followed by bath application of vehicle (ACSF) or CNO (5 μM) 4 weeks after virus injection. To assess whether vHPC input is required for the increased excitability in $CCK^{dmPFC→BLA}$ neurons during AOAT development, CCK-CreER mice received intra-BLA injection of AAV2/2-retro-Ef1α-DIO-EGFP (titer: 5.26×10^{12} genome copies/ml, 300 nl per side) and intra-vHPC injection of AAV2/9-CaMKII-hM4Di-mCherry (titer: 5.0×10^{12} genome copies/ml, 600 nl per side). Four weeks later, mice received daily CNO (1 mg/kg, intraperitoneally) injection in HC 10 min before morphine (5 mg/kg, intraperitoneally) injection for 3 days. Brain slices were obtained 30 min after the last morphine injection, and electrophysiological recordings were performed on visually identified $EGFP^+$ neurons in dmPFC. To assess interactions between MORs and CCK2Rs in BLA, electrophysiological recordings were obtained from visually identified BLA neurons in C57BL/6J mice following bath application of DAMGO (1 μM), CCK8s (1 μM) and L365260 (1 μM) as described in Fig. 7. To examine whether the endogenous CCK released from the $CCK^{dmPFC→BLA}$ terminals can antagonize the function of BLA MORs, four weeks after AAV-DIO-Ef1α-hM3Dq-mCherry (titer: 2.70×10^{12} genome copies/ml, 400 nl per side) unilateral injection, electrophysiological recordings were performed on visually identified BLA neurons in CCK-CreER mice followed by bath application of vehicle (ACSF), DAMGO (1 μM), CNO (5 μM), and L365260 (1 μM) as described in Fig. 7.

Recording of oEPSCs

For oEPSCs recordings, 473-nm blue laser light (15 mW/mm^2, 5-ms pulses, 20 Hz) was delivered by an optical fiber directly, and postsynaptic recording in voltage-clamp mode (holding potential, −70 mV) was performed in dmPFC with ChR2 terminal infection.

For electrophysiological recording of vHPC→dmPFC synaptic transmission, blue light was delivered to the dmPFC brain slices from C57BL/6J mice that received AAV2/9-Ef1α-hChR2 (H134R)-EYFP (titer: 2.00×10^{12} genome copies/ml, 400 nl per side) unilateral injection in vHPC. To study the vHPC→dmPFC→BLA projection, blue light was delivered to dmPFC mCherry$^+$ neurons from CCK-CreER mice in which vHPC had been unilaterally injected with AAV2/9-Ef1α-hChR2 (H134R)-EYFP (titer: 2.00×10^{12} genome copies/ml, 400 nl per side) and BLA had been unilaterally injected with AAV2/2-retro-Ef1α-DIO-mCherry (titer: 5.18×10^{12} genome copies/ml, 400 nl per side). NBQX (10 μM) and MK801 (10 μM) were used to examine whether the optically evoked postsynaptic currents are excitatory.

Recording of sEPSCs

sEPSCs were recorded under the voltage-clamp mode (holding potential, −70 mV) in the presence of 0.5 μM tetrodotoxin and 10 mM picrotoxin. To evaluate the effects of CNO on excitatory synaptic transmission, sEPSCs were recorded in dmPFC neurons from vGluT2-Cre mice in which vHPC had been injected with AAV2/9-Ef1α-DIO-hM3Dq-mCherry (titer: 2.70×10^{12} genome copies/ml, 600 nl per side) or AAV2/9-Ef1α-DIO-hM4Di-mCherry (titer: 5.55×10^{12} genome copies/ml, 600 nl per side) following bath application of vehicle (ACSF) and CNO (5 μM) four weeks after virus injection.

Drug administration and behavioral protocol

Intraperitoneal injection

For morphine or sufentanil intraperitoneal injection, all mice received intraperitoneal injection of morphine (1, 2.5, 5, and 10 mg/kg) or sufentanil (35 μg/kg) in HC or CC once daily for five consecutive days. For L365260 intraperitoneal injection, mice received intraperitoneal injection of L365260 (0.2 mg/kg) in HC 10 min before morphine injection once daily for four consecutive days. For CNO intraperitoneal injection, mice received intraperitoneal injection of CNO (1 mg/kg) in HC 10 min before morphine (5 mg/kg) injection once daily for five consecutive days. The hot-plate test was performed 15 min after morphine injection.

Intrathecal injection

For morphine intrathecal injection, awake mice were gently immobilized and dorsally shaved around the L4 and L5 vertebral segment area. Morphine (0.3 μg per mice) was subcutaneously injected into the L4-5 intervertebral space with a 20-gauge needle. Reflexive tail flick or "S" shape of the tail is a sign to identify successful intrathecal injection. After the injection, mice were placed in either HC or CC for 15 min followed by the hot-plate tests.

Intracranial drug infusion

Mice were handled for 5 to 10 min before experiments. A stainless steel injector attached to a 10-μl syringe (Hamilton) was inserted into the guide cannula after removing the cap. Drugs or vehicle (saline) were then infused (0.5 μl per side within 1 min) into the target brain area in the freely moving mice. The injector was slowly withdrawn 1 min after the infusion to allow the drug to diffuse, and the behavioral tests were performed roughly 25 min after the infusion. After the behavioral tests, the injection sites were confirmed by microinjection of Nissl dye. The data from mice with inaccurate injection sites were discarded.

Tamoxifen treatment

To induce the expression of Cre recombinase in CCK-CreER mice, tamoxifen (20 mg/ml; Sigma-Aldrich, T5648) was intraperitoneally injected daily at 100 μl/day for five consecutive days before any experiments. Tamoxifen was dissolved in sterile corn oil at room temperature and stored at 4°C.

Hot-plate and cold-plate tests

Before the experiment, mice were acclimatized to the hot/cold-plate test apparatus (Ugo Basile, Varese, Italy) for 3 days by placing them on plate at 22.5° ± 1°C for 5 min × 4 times daily. The plate surface was cleaned with 75% ethanol after each experiment. In the hot-plate test, mice were placed on the hot-plate at 52.5°C. The experiment was stopped as soon as the first observation of nocifensive behaviors, such as hind paw withdrawal or licking, stamping, and jumping. The time is recorded as paw withdrawal latency (PWL). All mice were tested, and the time was considered as pre-drug PWL. The cutoff time was 30 s to prevent tissue damage. After pre-drug PWL determination, the drugs were administered. Then, the pain threshold in the hot-plate tests after drug injection was measured as post-drug PWL. In the cold-plate test, mice were placed on the cold plate at 1°C, the experiment was stopped immediately when the ipsilateral hind paw of SNI-treated was first observed to brisk lift or stamp, and the cutoff time was 50 s. Then, pre-drug PWL and post-drug PWL were recorded. If the post-drug PWL reaches the cutoff time, it would be considered as maximum analgesic response. To analyze the analgesic efficacy, PWL was converted to the maximum possible effect (MPE). MPE was calculated using the following formula: MPE = [Post-drug PWL (s) − Pre-drug PWL (s)]/[Cutoff time (s) − Pre-drug PWL (s)]. To visualize the difference between groups, the MPE values were normalized to the day 1 values in each group, shown as normalized MPE. The raw PWL data for all experiments are presented in fig. S25.

AOAT test

Apparatus

AOAT was trained in HC and CC with a unique visual and tactile environment. The HC is a standard polycarbonate cage with woodchip bedding where mice were housed for at least two weeks. The CC is a rectangular chamber (19 cm × 19 cm × 24 cm) with black-and-white vertical stripe walls and smooth white plastic floor. After each experiment, the walls and floor of the CC were thoroughly cleaned with 75% ethanol.

Habituation period

Mice were handled once daily for 5 days before testing.

Experimental phase

The AOAT experiment lasted for 5 days. Mice were randomly divided into two groups: the HC group and the CC group. The HC-mice and the CC-mice were placed on a hot plate (52.5°C) to measure their basal pain threshold. After baseline measurements, the HC-mice received intraperitoneal injections of morphine (1, 2.5, and 5 mg/kg) and then immediately placed back to their home cages. Fifteen minutes later, the post-drug PWL was measured by hot-plate tests (the pain measurement takes no more than 30 s), after which the HC-mice were returned to their home cages. After the baseline measurements, the CC-mice received intraperitoneal injections of morphine and were then immediately placed into the context chamber for 15 min, followed by the hot-

plate test. After the test, the CC-mice were immediately placed back into the CC for another 75 min and then returned to their home cage.

Chronic inflammatory pain

In the CFA-induced inflammatory pain model, 20 μl of 50% CFA was subcutaneously injected into the plantar surface of the mouse hind paws after the baseline measurements. Hot-plate tests were repeated daily after CFA injection for 7 days (days 1 to 7). CFA-treated mice developed significantly reduced PWL, and the mice with no reduced PWL were discarded. The AOAT training started from day 3.

SNI surgery

After the baseline measurement, mice were deeply anesthetized with an intraperitoneal injection of pentobarbital sodium (80 mg/kg), and the left sciatic nerves (including tibial nerves, common peroneal nerves, and sural nerves) were exposed in the mid-thigh. The tibial and common peroneal nerves were tightly ligated with a 5.0 silk and transected distally, whereas the sural nerve was kept intact. After surgery, the muscle and skin were closed in two layers and mice were returned to HC. Cold-plate tests (1°C) were performed 4 days postoperatively, and AOAT training was started.

Morphine-induced respiratory depression

Respiratory measurement

By using the MouseOx Plus System (STARR Life Science, USA), we measured the respiratory rate of anesthetized mice. Briefly, mice were shaved the necks and the CollarClip sensor was applied from the back of the neck of the mice, and the respiratory rate was collected via MouseOx Plus software. Respiratory rates were reported on the software screen and calculated in 1-min bins to obtain the average respiratory rate. To quantify the morphine-induced respiratory depression, two time periods, 5 min before morphine injection and 30 to 40 min after morphine injection, were analyzed. Morphine-induced respiratory depression was calculated using the following formula: [respiratory rate after morphine injection (breaths per minute, bpm) − respiratory rate of baseline (bpm)]/[respiratory rate of baseline (bpm)].

One day before the experiment, mice were lightly anesthetized by isoflurane and the neck hair was shaved. Mice were then acclimatized to the CollarClip sensors and maintained a stable respiratory rate of 100 to 150 bpm for 1 hour. During the experiment, mice were kept under isoflurane anesthesia until the respiratory rate stabilized and the respiratory rates were recorded for 5 min. Twenty minutes after the baseline measurement, mice were systemically injected with morphine (10 mg/kg, intraperitoneally) in HC and CC. Thirty minutes later, mice were anesthetized and respiratory rates were recorded for 10 min in HC and CC, after which the CC-mice stayed at CC for another 60 min before returning to their home cage.

Tissue staining

Tissue preparation

Mice were deeply anesthetized with an intraperitoneal injection of pentobarbital sodium (80 mg/kg) and perfused transcardially with ice-cold phosphate-buffered saline (PBS; pH 7.4) followed by 4% paraformaldehyde solution (PFA; dissolved in PBS, pH 7.4). After perfusion, brains were extracted and postfixed overnight in 4% PFA at 4°C with cryoprotection in 30% sucrose. Coronal slices (40 μm) were prepared using a freezing microtome (Leica CM 1860).

Immunofluorescent staining

Tissue sections were incubated in 0.3% Triton X-100 for 20 min and then blocked with 10% goat serum for 45 min at room temperature (20° to 23°C). The sections were incubated with primary antibodies, including anti–c-Fos (1:1000; Abcam, ab190289), anti-MOR (1:300; EMD Millipore, AB5509), anti-CCK2R (1:500; Alomone Labs, ACR-042), anti-CCK8s (1:300; IMMUNOSTAR, 20078), anti-NeuN (1:1000; Sigma-Aldrich, MAB377), and anti-CaMKII (1:250; Abcam, ab22609) at 4°C for 24 hours. After the incubation with primary antibodies, sections were washed with PBS (5 × 8 min) and then incubated with corresponding fluorophore-conjugated secondary antibodies, including Alexa Fluor 594 goat anti-rabbit (1:500; Cell Signaling Technology, 8889S), Alexa Fluor 594 goat anti-pig (1:300; Invitrogen, A11075), Alexa Fluor 488 goat anti-mouse (1:500; Cell Signaling Technology, 4880S), Alexa Fluor 488 goat anti-rabbit (1:500; Cell Signaling Technology, 4412S), and Alexa Fluor 594 goat anti-mouse (1:500; Cell Signaling Technology, 8890S) for 2 hours at room temperature. For c-Fos immunostaining, HC-mice and CC-mice were anesthetized in the HC and CC 90 min after the last morphine injection on day 5, respectively, followed by transcardially perfusion. Brian slices were examined and photographed using an LSM 880 (Zeiss, Germany) confocal microscope.

3,3′-Diaminobenzidine staining

The sections were blocked with 0.3% H_2O_2 (in methanol) for 30 min, incubated in 0.3% Triton X-100 for 15 min, and blocked with 10% goat serum for 1 hour at room temperature. Next, sections were incubated with primary antibody of anti-MOR (1:100; Abcam, ab10275) for 48 hours at 4°C, followed by second antibody of biotinylated goat anti-rabbit immunoglobulin G (1:200; Vector, PK-6101) for 2 hours at room temperature. After incubation with avidin-biotin complex (Vector, PK-6101) for 30 min at 37°C, sections were incubated in DAB (3,3′-diaminobenzidine)–ammonium nickel sulfate developing solution (Vector, SK-4100). Last, ethyl ethanol and xylene were used for decoloration and mounted with Neutral Balsam (Sangon Biotech, E675007).

Quantitative real-time PCR assay

For the *Oprm1* mRNA assay, the BLA region in the brain of $Oprm1^{fl/fl}$ mice was harvested four weeks after AAV2/9-hSyn-Cre-EGFP (titer: 3.21×10^{12} genome copies/ml, 400 nl per side) or AAV2/9-hSyn-EGFP (titer: 2.05×10^{12} genome copies/ml, 400 nl per side) bilateral injection. For the *CCK* mRNA assay, the dmPFC region in the brain of C57BL/6J mice was harvested 4 hours after morphine injections. Total RNA was extracted using TRIzol (Life Technologies). RNA purity, integrity, and concentration were determined, and 100 to 200 ng of total RNA were reversely transcribed to complementary DNA (cDNA) using the HiScript II Strand cDNA Synthesis Kit (Vazyme). qRT-PCR was performed on the LightCycler 96 Instrument System using AceQ qPCR SYBR Green Master Mix (Vazyme). Melt curves were analyzed to verify the amplicon specificity. All qRT-PCRs were conducted in technical triplicates, and the results were averaged for each sample, normalized to the mean housekeeping messenger RNA expression levels, and analyzed using the method of $2^{-\Delta CT}$. The sequences of the PCR primers were as follows: for *GAPDH*, 5′-AGGTCGGTGTGAACGGATTTG-3′ and 5′-TGTAGACCATGTAGTTGAGGTCA-3′; for *Oprm1*, 5′-ATCCTCTCTTCTGCCATTGGT-3′ and 5′-

TGAAGGCGAAGATGAAGACA-3′; for *CCK*, 5′-GCACTGCTAGCGCGATACATC-3′ and 5′-CCAGGCTCTGCAGGTTCTTAAG-3′.

Transcriptome and gene expression analyses

Total RNA was extracted from frozen dmPFC brain tissue of C57/BL6J mice after 5 days of repeated morphine injections using TRIzol (Invitrogen) according to manual instructions. The cDNA libraries were prepared and sequenced on the BGIseq500 platform (Beijing Genomic Institute in Shenzhen). The total number of reads that were obtained for each sample was approximately 6 gb. The sequence data were processed and mapped to the *Mus musculus* reference genome using Bowtie2 (v2.2.5) (*76*). Gene expression was quantified to the fragments per kilobase million (FPKM) using RNA-seq by expectation-maximization (RSEM).

Calcium imaging studies

Virus injection

For imaging in vivo calcium transients of the BLA-projecting dmPFC neurons, AAV2/2-retro-hSyn-Cre (titer: 5.51×10^{12} genome copies/ml, 400 nl per side) was unilaterally injected into BLA, and AAV2/9-Ef1α-DIO-GCaMP6f-tdTomato (titer: 6.46×10^{12} genome copies/ml, 400 nl per side) or AAV2/9-Ef1α-DIO-GCaMP7f-tdTomato (titer: 3.36×10^{12} genome copies/ml, 400 nl per side) was unilaterally injected into dmPFC. Three weeks later, mice were implanted with a microendoscope lens (AP, +2.10 mm; ML, +0.30 mm; DV, −0.75 mm). AAV-Ef1α-DIO-GCaMP6f-tdTomato and AAV2/9-Ef1α-DIO-GCaMP7f-tdTomato were obtained from OBiO Technology, Shanghai, China.

GRIN lens implantation

At three weeks following virus injection, a 1-mm-diameter gradient refractive index (GRIN) lens was implanted to the injection site in dmPFC based on the protocols of the previous study (*77*). The mouse was anesthetized and mounted on the stereotaxic apparatus. A 1.1-mm-diameter circular craniotomy was centered at the following coordinates: AP: +2.10 mm; ML: +0.3 mm relative to bregma. ACSF was repeatedly applied to the brain to avoid drying, and the brain cortex above dmPFC was slowly aspirated using a 30-gauge blunted needle attached to accustom-constructed three-axis motorized robotic arm controlled by MATLAB-based software (https://github.com/liang-bo/AutoStereota). The GRIN lens was slowly lowered to dmPFC to a depth of −0.75 mm relative to the brain surface and then was secured to the skull using dental cement. Meanwhile, the miniscope base was fixed to the mouse head using dental cement. During recovery, the exposed lens was protected by a protective cap.

Calcium signal acquisition

Four weeks after virus injection, a miniscope (*78*) with a blue light-emitting diode power (0.1 to 0.3 mW, 465 nm) was mounted onto the mouse head and adjusted to obtain the best position to visualize the GCaMP calcium indicator. All calcium recordings were acquired at 10-Hz frame rate. Before the behavioral experiments, mice were habituated to the miniscope attachment procedure and experimenter for 2 to 3 days. To avoid the acute effect of the calcium imaging recording process, the miniscope was always attached to the mice during the 5-day behavioral training. On day 6, mice were hooked up to the miniscope and placed in the HC and CC for 10 min sequentially. The dmPFC calcium signal was recorded during the total 20 min.

Imaging data analysis

Calcium imaging data were analyzed in MATLAB (MathWorks, USA). Calcium imaging data of individual sessions were concatenated and spatially downsampled by a custom software (Neu View) that was developed in C++ to communicate with the data acquisition controller (*77*). To correct the artifacts caused by movement, we performed a motion correction by an open-source script described in a previous study (*79*). Then, we cropped black borders around regions of interest (ROIs) to avoid error detection by high-contrast borders. We applied the extended constrained nonnegative matrix factorization (*80*) to detect neurons, extract calcium signal traces ($\Delta F/F$), and ROIs. Calcium traces were normalized to z score (x-$\text{mean}_{\Delta F/F}$)/$\text{std}_{\Delta F/F}$) for further analysis. For Ca^{2+} heatmaps by time, calcium traces were binarized by its average individually. Calcium events were marked by the peak z score values using a customized MATLAB script.

Drugs

Most chemicals such as NBQX and MK801 were achieved from Sigma-Aldrich. Morphine hydrochloride was achieved from Shenyang Pharmaceutical Co. Ltd. under surveillance of Chinese Food and Drug Administration; sufentanil citrate was achieved from Renfu Pharmaceutical Co. Ltd. under surveillance of Chinese Food and Drug Administration; naloxone hydrochloride was achieved from Chongqing Lummy Pharmaceutical Co. Ltd.; CTOP was achieved from Abcam; naltrindole, nor-BNI, CCK8s, L365260, MK329, DAMGO, and CNO were achieved from Tocris. All drugs were first dissolved to a maximum concentration according to the manufacturer's instructions, and the final solutions were prepared immediately before experiments.

Statistical analysis

Statistical analysis was performed using GraphPad Prism 7.0 (GraphPad Software). Statistical differences of data were determined using paired or unpaired Student's t test for two-group comparisons, and one-way or two-way analysis of variance (ANOVA) followed by Bonferroni post hoc test for multiple comparisons as indicated in all figure legends. No statistical methods were used to predetermine sample size, but our sample sizes were similar to those reported by previous reporters. All data are presented as the means ± SEM, and significance levels are indicated as $^{*}P < 0.05$, $^{**}P < 0.01$, and $^{***}P < 0.001$.

Supplementary Materials

This PDF file includes:
Figs. S1 to S25

Other Supplementary Material for this manuscript includes the following:
Movie S1

REFERENCES AND NOTES

1. C. Blanco, N. D. Volkow, Management of opioid use disorder in the USA: Present status and future directions. *Lancet* **393**, 1760–1772 (2019).
2. S. Mercadante, E. Bruera, Opioid switching: A systematic and critical review. *Cancer Treat. Rev.* **32**, 304–315 (2006).
3. S. Majumdar, L. A. Devi, Strategy for making safer opioids bolstered. *Nature* **553**, 286–288 (2018).

4. N. D. Volkow, E. B. Jones, E. B. Einstein, E. M. Wargo, Prevention and treatment of opioid misuse and addiction: A review. *JAMA Psychiat.* **76**, 208–216 (2019).
5. C. Buntin-Mushock, L. Phillip, K. Moriyama, P. P. Palmer, Age-dependent opioid escalation in chronic pain patients. *Anesth. Analg.* **100**, 1740–1745 (2005).
6. J. A. J. Martyn, J. Mao, E. A. Bittner, Opioid tolerance in critical illness. *N. Engl. J. Med.* **380**, 365–378 (2019).
7. M. M. Morgan, M. J. Christie, Analysis of opioid efficacy, tolerance, addiction and dependence from cell culture to human. *Br. J. Pharmacol.* **164**, 1322–1334 (2011).
8. K. M. Raehal, C. L. Schmid, C. E. Groer, L. M. Bohn, Functional selectivity at the μ-opioid receptor: Implications for understanding opioid analgesia and tolerance. *Pharmacol. Rev.* **63**, 1001–1019 (2011).
9. P. Y. Law, P. H. Reggio, H. H. Loh, Opioid receptors: Toward separation of analgesic from undesirable effects. *Trends Biochem. Sci.* **38**, 275–282 (2013).
10. B. L. Kieffer, C. J. Evans, Opioid tolerance-in search of the holy grail. *Cell* **108**, 587–590 (2002).
11. C. M. Cahill, W. Walwyn, A. M. W. Taylor, A. A. A. Pradhan, C. J. Evans, Allostatic mechanisms of opioid tolerance beyond desensitization and downregulation. *Trends Pharmacol. Sci.* **37**, 963–976 (2016).
12. G. Corder, V. L. Tawfik, D. Wang, E. I. Sypek, S. A. Low, J. R. Dickinson, C. Sotoudeh, J. D. Clark, B. A. Barres, C. J. Bohlen, G. Scherrer, Loss of μ opioid receptor signaling in nociceptors, but not microglia, abrogates morphine tolerance without disrupting analgesia. *Nat. Med.* **23**, 164–173 (2017).
13. E. Gibula-Tarlowska, J. H. Kotlinska, Crosstalk between opioid and anti-opioid systems: An overview and its possible therapeutic significance. *Biomolecules* **10**, 1376 (2020).
14. S. Siegel, Evidence from rats that morphine tolerance is a learned response. *J. Comp. Psychol.* **89**, 498–506 (1975).
15. S. T. Tiffany, D. J. Drobes, A. Cepeda-Benito, Contribution of associative and nonassociative processes to the development of morphine tolerance. *Psychopharmacology* **109**, 185–190 (1992).
16. J. M. Mitchell, A. I. Basbaum, H. L. Fields, A locus and mechanism of action for associative morphine tolerance. *Nat. Neurosci.* **3**, 47–53 (2000).
17. J. L. Azorlosa, N. E. Hartley, C. Deffner-Rappold, Context-specific morphine tolerance and withdrawal: The effects of interdose interval. *Psychobiology* **22**, 304–311 (1994).
18. S. Siegel, R. E. Hinson, M. D. Krank, J. McCully, Heroin "overdose" death: Contribution of drug-associated environmental cues. *Science* **216**, 436–437 (1982).
19. M. Kavaliers, M. Hirst, Environmental specificity of tolerance to morphine-induced analgesia in a terrestrial snail: Generalization of the behavioral model of tolerance. *Pharmacol. Biochem. Behav.* **25**, 1201–1206 (1986).
20. P. Schnur, R. A. Martinez, Environmental control of morphine tolerance in the hamster. *Anim. Learn. Behav.* **17**, 322–327 (1989).
21. S. Siegel, Pavlovian conditioning and drug overdose: When tolerance fails. *Addict. Res. Theory* **9**, 503–513 (2001).
22. S. Siegel, D. W. Ellsworth, Pavlovian conditioning and death from apparent overdose of medically prescribed morphine: A case report. *Bull. Psychon. Soc.* **24**, 278–280 (1986).
23. J. Gerevich, E. Bácskai, L. Farkas, Z. Danics, A case report: Pavlovian conditioning as a risk factor of heroin 'overdose' death. *Harm Reduct. J.* **2**, 11 (2005).
24. S. Siegel, Pavlovian conditioning and heroin overdose: Reports by overdose victims. *Bull. Psychon. Soc.* **22**, 428–430 (1984).
25. P. L. Faris, B. R. Komisaruk, L. R. Watkins, D. J. Mayer, Evidence for the neuropeptide cholecystokinin as an antagonist of opiate analgesia. *Science* **219**, 310–312 (1983).
26. C. Gall, J. Lauterborn, D. Burks, K. Seroogy, Co-localization of enkephalin and cholecystokinin in discrete areas of rat brain. *Brain Res.* **403**, 403–408 (1987).
27. M. Pohl, J. J. Benoliel, S. Bourgoin, M. C. Lombard, A. Mauborgne, H. Taquet, A. Carayon, J. M. Besson, F. Cesselin, M. Hamon, Regional distribution of calcitonin gene-related peptide-, substance P-, cholecystokinin-, Met5-enkephalin-, and dynorphin A (1–8)-like materials in the spinal cord and dorsal root ganglia of adult rats: Effects of dorsal rhizotomy and neonatal capsaicin. *J. Neurochem.* **55**, 1122–1130 (1990).
28. X. J. Wang, S. G. Fan, M. F. Ren, J. S. Han, Cholecystokinin-8 suppressed 3H-etorphine binding to rat brain opiate receptors. *Life Sci.* **45**, 117–123 (1989).
29. X. J. Wang, J. S. Han, Modification by cholecystokinin octapeptide of the binding of mu-, delta-, and kappa-opioid receptors. *J. Neurochem.* **55**, 1379–1382 (1990).
30. S. Itoh, G. Katsuura, Y. Maeda, Caerulein and cholecystokinin suppress beta-endorphin-induced analgesia in the rat. *Eur. J. Pharmacol.* **80**, 421–425 (1982).
31. D. S. Magnuson, A. F. Sullivan, G. Simonnet, B. P. Roques, A. H. Dickenson, Differential interactions of cholecystokinin and FLFQPQRF-NH2 with mu and delta opioid antinociception in the rat spinal cord. *Neuropeptides* **16**, 213–218 (1990).
32. M. F. O'Neill, C. T. Dourish, S. D. Iversen, Morphine-induced analgesia in the rat paw pressure test is blocked by CCK and enhanced by the CCK antagonist MK-329. *Neuropharmacology* **28**, 243–247 (1989).
33. C. T. Dourish, D. Hawley, S. D. Iversen, Enhancement of morphine analgesia and prevention of morphine tolerance in the rat by the cholecystokinin antagonist L-364,718. *Eur. J. Pharmacol.* **147**, 469–472 (1988).
34. X. Z. Ding, S. G. Fan, J. P. Zhou, J. S. Han, Reversal of tolerance to morphine but no potentiation of morphine-induced analgesia by antiserum against cholecystokinin octapeptide. *Neuropharmacology* **25**, 1155–1160 (1986).
35. R. Maldonado, M. Derrien, F. Noble, B. P. Roques, Association of the peptidase inhibitor RB 101 and a CCK-B antagonist strongly enhances antinociceptive responses. *Neuroreport* **4**, 947–950 (1993).
36. G. J. McCleane, A phase 1 study of the cholecystokinin (CCK) B antagonist L-365,260 in human subjects taking morphine for intractable non-cancer pain. *Neurosci. Lett.* **332**, 210–212 (2002).
37. V. Tortorici, L. Nogueira, R. Salas, H. Vanegas, Involvement of local cholecystokinin in the tolerance induced by morphine microinjections into the periaqueductal gray of rats. *Pain* **102**, 9–16 (2003).
38. L. R. Watkins, I. B. Kinscheck, D. J. Mayer, Potentiation of opiate analgesia and apparent reversal of morphine tolerance by proglumide. *Science* **224**, 395–396 (1984).
39. L. R. Watkins, I. B. Kinscheck, E. F. S. Kaufman, J. Miller, H. Frenk, D. J. Mayer, Cholecystokinin antagonists selectively potentiate analgesia induced by endogenous opiates. *Brain Res.* **327**, 181–190 (1985).
40. J. Y. Xie, D. S. Herman, C. O. Stiller, L. R. Gardell, M. H. Ossipov, J. Lai, F. Porreca, T. W. Vanderah, Cholecystokinin in the rostral ventromedial medulla mediates opioid-induced hyperalgesia and antinociceptive tolerance. *J. Neurosci.* **25**, 409–416 (2005).
41. X. J. Xu, Z. Wiesenfeld-Hallin, J. Hughes, D. C. Horwell, T. Hökfelt, CI988, a selective antagonist of cholecystokininB receptors, prevents morphine tolerance in the rat. *Br. J. Pharmacol.* **105**, 591–596 (1992).
42. X. Zhu, H.-D. Tang, W.-Y. Dong, F. Kang, A. Liu, Y. Mao, W. Xie, X. Zhang, P. Cao, W. Zhou, H. Wang, Z. Farzinpour, W. Tao, X. Song, Y. Zhang, T. Xue, Y. Jin, J. Li, Z. Zhang, Distinct thalamocortical circuits underlie allodynia induced by tissue injury and by depression-like states. *Nat. Neurosci.* **24**, 542–553 (2021).
43. G. Corder, D. C. Castro, M. R. Bruchas, G. Scherrer, Endogenous and exogenous opioids in pain. *Annu. Rev. Neurosci.* **41**, 453–473 (2018).
44. Q. Wang, Q. Wang, X. L. Song, Q. Jiang, Y. J. Wu, Y. Li, T. F. Yuan, S. Zhang, N. J. Xu, M. X. Zhu, W. G. Li, T. L. Xu, Fear extinction requires ASIC1a-dependent regulation of hippocampal-prefrontal correlates. *Sci. Adv.* **4**, eaau3075 (2018).
45. R. C. Twining, K. Lepak, A. J. Kirry, M. R. Gilmartin, Ventral hippocampal input to the prelimbic cortex dissociates the context from the cue association in trace fear memory. *J. Neurosci.* **40**, 3217–3230 (2020).
46. F. Sotres-Bayon, D. Sierra-Mercado, E. Pardilla-Delgado, G. J. Quirk, Gating of fear in prelimbic cortex by hippocampal and amygdala inputs. *Neuron* **76**, 804–812 (2012).
47. S. P. Jadhav, G. Rothschild, D. K. Roumis, L. M. Frank, Coordinated excitation and inhibition of prefrontal ensembles during awake hippocampal sharp-wave ripple events. *Neuron* **90**, 113–127 (2016).
48. J. R. Monforte, Some observations concerning blood morphine concentrations in narcotic addicts. *J. Forensic Sci.* **22**, 718–724 (1977).
49. J. M. White, R. J. Irvine, Mechanisms of fatal opioid overdose. *Addiction* **94**, 961–972 (1999).
50. S. Ortiz, M. S. Latsko, J. L. Fouty, S. Dutta, J. M. Adkins, A. M. Jasnow, Anterior cingulate cortex and ventral hippocampal inputs to the basolateral amygdala selectively control generalized fear. *J. Neurosci.* **39**, 6526–6539 (2019).
51. W.-Z. Liu, W.-H. Zhang, Z.-H. Zheng, J.-X. Zou, X.-X. Liu, S.-H. Huang, W.-J. You, Y. He, J.-Y. Zhang, X.-D. Wang, B.-X. Pan, Identification of a prefrontal cortex-to-amygdala pathway for chronic stress-induced anxiety. *Nat. Commun.* **11**, 2221 (2020).
52. R. Marek, L. Xu, R. K. P. Sullivan, P. Sah, Excitatory connections between the prelimbic and infralimbic medial prefrontal cortex show a role for the prelimbic cortex in fear extinction. *Nat. Neurosci.* **21**, 654–658 (2018).
53. J. H. Cho, K. Deisseroth, V. Y. Bolshakov, Synaptic encoding of fear extinction in mPFC-amygdala circuits. *Neuron* **80**, 1491–1507 (2013).
54. S. L. Resendez, J. H. Jennings, R. L. Ung, V. M. K. Namboodiri, Z. C. Zhou, J. M. Otis, H. Nomura, J. A. McHenry, O. Kosyk, G. D. Stuber, Visualization of cortical, subcortical and deep brain neural circuit dynamics during naturalistic mammalian behavior with head-mounted microscopes and chronically implanted lenses. *Nat. Protoc.* **11**, 566–597 (2016).
55. P. Sah, E. S. Faber, M. Lopez De Armentia, J. Power, The amygdaloid complex: Anatomy and physiology. *Physiol. Rev.* **83**, 803–834 (2003).
56. S. Duvarci, D. Pare, Amygdala microcircuits controlling learned fear. *Neuron* **82**, 966–980 (2014).
57. X.-Y. Zhang, Y.-N. Dou, L. Yuan, Q. Li, Y.-J. Zhu, M. Wang, Y.-G. Sun, Different neuronal populations mediate inflammatory pain analgesia by exogenous and endogenous opioids. *eLife* **9**, e55289 (2020).

58. M. Dufresne, C. Seva, D. Fourmy, Cholecystokinin and gastrin receptors. *Physiol. Rev.* **86**, 805–847 (2006).
59. C. K. Hwang, D. K. Kim, H. S. Chun, Cholecystokinin-8 induces brain-derived neurotrophic factor expression in noradrenergic neuronal cells. *Neuropeptides* **47**, 245–250 (2013).
60. J. Arthur, E. Bruera, Balancing opioid analgesia with the risk of nonmedical opioid use in patients with cancer. *Nat. Rev. Clin. Oncol.* **16**, 213–226 (2019).
61. C. A. Verberkt, M. H. J. van den Beuken-van Everdingen, J. M. G. A. Schols, N. Hameleers, E. F. M. Wouters, D. J. A. Janssen, Effect of sustained-release morphine for refractory breathlessness in chronic obstructive pulmonary disease on health status: A randomized clinical trial. *JAMA Intern. Med.* **180**, 1306–1314 (2020).
62. E. Bandieri, M. Romero, C. I. Ripamonti, F. Artioli, D. Sichetti, C. Fanizza, D. Santini, L. Cavanna, B. Melotti, P. F. Conte, F. Roila, S. Cascinu, E. Bruera, G. Tognoni, M. Luppi; Early Strong Opioid Treatment Study (ESOT) Investigators, Randomized trial of low-dose morphine versus weak opioids in moderate cancer pain. *J. Clin. Oncol.* **34**, 436–442 (2016).
63. H. Eichenbaum, Prefrontal–hippocampal interactions in episodic memory. *Nat. Rev. Neurosci.* **18**, 547–558 (2017).
64. K. A. Corcoran, G. J. Quirk, Activity in prelimbic cortex is necessary for the expression of learned, but not innate, Fears. *J. Neurosci.* **27**, 840–844 (2007).
65. J. C. Jimenez, K. Su, A. R. Goldberg, V. M. Luna, J. S. Biane, G. Ordek, P. Zhou, S. K. Ong, M. A. Wright, L. Zweifel, L. Paninski, R. Hen, M. A. Kheirbek, Anxiety cells in a hippocampal-hypothalamic circuit. *Neuron* **97**, 670–683.e6 (2018).
66. R. Place, A. Farovik, M. Brockmann, H. Eichenbaum, Bidirectional prefrontal-hippocampal interactions support context-guided memory. *Nat. Neurosci.* **19**, 992–994 (2016).
67. C. Kibaly, C. Xu, C. M. Cahill, C. J. Evans, P. Y. Law, Non-nociceptive roles of opioids in the CNS: Opioids' effects on neurogenesis, learning, memory and affect. *Nat. Rev. Neurosci.* **20**, 5–18 (2019).
68. J. D. Levine, N. C. Gordon, H. L. Fields, The mechanism of placebo analgesia. *Lancet* **2**, 654–657 (1978).
69. G. Miguez, M. A. Laborda, R. R. Miller, Classical conditioning and pain: Conditioned analgesia and hyperalgesia. *Acta Psychol. (Amst)* **145**, 10–20 (2014).
70. S. A. Tershner, F. J. Helmstetter, Antinociception produced by mu opioid receptor activation in the amygdala is partly dependent on activation of mu opioid and neurotensin receptors in the ventral periaqueductal gray. *Brain Res.* **865**, 17–26 (2000).
71. F. J. Helmstetter, P. S. F. Bellgowan, L. H. Poore, Microinfusion of mu but not delta or kappa opioid agonists into the basolateral amygdala results in inhibition of the tail flick reflex in pentobarbital-anesthetized rats. *J. Pharmacol. Exp. Ther.* **275**, 381–388 (1995).
72. S. McGaraughty, M. M. Heinricher, Microinjection of morphine into various amygdaloid nuclei differentially affects nociceptive responsiveness and RVM neuronal activity. *Pain* **96**, 153–162 (2002).
73. P. L. Faris, C. L. McLaughlin, C. A. Baile, J. W. Olney, B. R. Komisaruk, Morphine analgesia potentiated but tolerance not affected by active immunization against cholecystokinin. *Science* **226**, 1215–1217 (1984).
74. L. Medrihan, Y. Sagi, Z. Inde, O. Krupa, C. Daniels, A. Peyrache, P. Greengard, Initiation of behavioral response to antidepressants by cholecystokinin neurons of the dentate gyrus. *Neuron* **95**, 564–576.e4 (2017).
75. T. Matsuda, T. Y. Hiyama, K. Kobayashi, K. Kobayashi, M. Noda, Distinct CCK-positive SFO neurons are involved in persistent or transient suppression of water intake. *Nat. Commun.* **11**, 5692 (2020).
76. B. Li, C. N. Dewey, RSEM: Accurate transcript quantification from RNA-Seq data with or without a reference genome. *BMC Bioinformatics* **12**, 323 (2011).
77. L. Zhang, B. Liang, G. Barbera, S. Hawes, Y. Zhang, K. Stump, I. Baum, Y. Yang, Y. Li, D. T. Lin, Miniscope GRIN lens system for calcium imaging of neuronal activity from deep brain structures in behaving animals. *Curr. Protoc. Neurosci.* **86**, e56 (2019).
78. G. Barbera, B. Liang, L. Zhang, C. R. Gerfen, E. Culurciello, R. Chen, Y. Li, D. T. Lin, Spatially compact neural clusters in the dorsal striatum encode locomotion relevant information. *Neuron* **92**, 202–213 (2016).
79. E. A. Pnevmatikakis, A. Giovannucci, NoRMCorre: An online algorithm for piecewise rigid motion correction of calcium imaging data. *J. Neurosci. Methods* **291**, 83–94 (2017).
80. P. Zhou, S. L. Resendez, J. Rodriguez-Romaguera, J. C. Jimenez, S. Q. Neufeld, A. Giovannucci, J. Friedrich, E. A. Pnevmatikakis, G. D. Stuber, R. Hen, M. A. Kheirbek, B. L. Sabatini, R. E. Kass, L. Paninski, Efficient and accurate extraction of in vivo calcium signals from microendoscopic video data. *eLife* **7**, (2018).

Acknowledgments: We thank Y. Sun (Institute of Neuroscience, Chinese Academy of Sciences) for providing transgenic mouse lines and H. Wang (Anhui Medical University) and Key Laboratory of Environmental Toxicology of Anhui Higher Education Institutes for providing MouseOx Plus system. **Funding:** This work was funded by National Key R&D Program of China grant 2021YFA0804900 (W.X.); National Natural Science Foundation of China grants 32225020, 91849206, 91649121, 91942315, 92049304, and 32121002 to W.X. and 81901157, and 82241032 to G.Z.; Strategic Priority Research Program of the Chinese Academy of Sciences grant XDB39050000 (W.X.); Key Research Program of Frontier Science grant no. ZDBS-LY-SM002 (W.X.); CAS Interdisciplinary Innovation Team grant JCTD-2018-20 (W.X.); The Youth Innovation Promotion Association CAS (W.X.); CAS Collaborative Innovation Program of Hefei Science Center 2021HSC-CIP003 (W.X.); Fundamental Research Funds for the Central Universities, USTC Research Funds of the Double First-Class Initiative grant YD9100002001 (W.X.); CAS Project for Young Scientists in Basic Research grant YSBR-013 (W.X.); and China Postdoctoral Science Foundation grant 2020TQ0314 (G.Z.). **Author contributions:** Conceptualization: W.X. Methodology: Y.H., H.G., G.Z., X.W., X.M., X.C., Z.X., X.Z., J.X., H.M., M.Y., Q.C., P.C., and Y.Y. Investigation: Y.H., G.Z., W.X., and L.Z. Visualization: Y.H. Funding acquisition: W.X. Project administration: W.X. Supervision: W.X. Writing—original draft: W.X., Y.H., G.Z., and L.Z. Writing—review and editing: W.X., Y.H., G.Z., and L.Z. **Competing interests:** The authors declare that they have no competing interests. **Data and materials availability:** All data needed to evaluate the conclusions in the paper are present in the paper and/or the Supplementary Materials. Raw RNA-seq data were deposited in the sequence read archive (SRA) at the NCBI (accession number PRJNA867538, www.ncbi.nlm.nih.gov/bioproject/PRJNA867538).

Submitted 10 February 2022
Accepted 22 December 2022
Published 8 February 2023
10.1126/sciadv.abo5627